

VARIATIONS IN THE PEAK POSITION OF THE 6.2 μm INTERSTELLAR EMISSION FEATURE: A TRACER OF N IN THE INTERSTELLAR POLYCYCLIC AROMATIC HYDROCARBON POPULATION

DOUGLAS M. HUDGINS,^{1,2} CHARLES W. BAUSCHLICHER, JR.,³ AND L. J. ALLAMANDOLA¹

Received 2005 January 31; accepted 2005 May 31

ABSTRACT

This paper presents the results of an investigation of the molecular characteristics that underlie the observed peak position and profile of the nominal 6.2 μm interstellar emission band generally attributed to the CC stretching vibrations of polycyclic aromatic hydrocarbons (PAHs). It begins with a summary of recent experimental and theoretical studies of the spectroscopic properties of large (>30 carbon atoms) PAH cations as they relate to this aspect of the astrophysical problem. It then continues with an examination of the spectroscopic properties of a number of PAH variants within the context of the interstellar 6.2 μm emission, beginning with a class of compounds known as polycyclic aromatic nitrogen heterocycles (PANHs; PAHs with one or more nitrogen atoms substituted into their carbon skeleton). In this regard, we summarize the results of recent relevant experimental studies involving a limited set of small PANHs and their cations and then report the results of a comprehensive computational study that extends that work to larger PANH cations including many nitrogen-substituted variants of coronene⁺ (C₂₄H₁₂⁺), ovalene⁺ (C₃₂H₁₄⁺), circumcoronene⁺ (C₅₄H₁₈⁺), and circum-circumcoronene⁺ (C₉₆H₂₄⁺). Finally, we report the results of more focused computational studies of selected representatives from a number of other classes of PAH variants that share one or more of the key attributes of the PANH species studied. These alternative classes of PAH variants include (1) oxygen- and silicon-substituted PAH cations; (2) PAH-metal ion complexes (metallocenes) involving the cosmically abundant elements magnesium and iron; and (3) large, asymmetric PAH cations.

Overall, the studies reported here demonstrate that increasing PAH size alone is insufficient to account for the position of the shortest wavelength interstellar 6.2 μm emission bands, as had been suggested by earlier studies. On the other hand, this work reveals that substitution of one or more nitrogen atoms within the interior of the carbon skeleton of a PAH cation induces a significant blueshift in the position of the dominant CC stretching feature of these compounds that is sufficient to account for the position of the interstellar bands. Subsequent studies of the effects of substitution by other heteroatoms (O and Si), metal ion complexation (Fe⁺, Mg⁺, and Mg²⁺), and molecular symmetry variation—all of which fail to reproduce the blueshift observed in the PANH cations—indicate that N appears to be unique in its ability to accommodate the position of the interstellar 6.2 μm bands while simultaneously satisfying the other constraints of the astrophysical problem. This result implies that the peak position of the interstellar feature near 6.2 μm traces the degree of nitrogen substitution in the population, that most of the PAHs responsible for the interstellar IR emission features incorporate nitrogen within their aromatic networks, and that a lower limit of 1%–2% of the cosmic nitrogen is sequestered within the interstellar PAH population.

Finally, in view of the ubiquity and abundance of interstellar PAHs and the permanent dipoles and distinctive electronic structures of these nitrogen-substituted variants, this work impacts a wide range of observational phenomena outside of the infrared region of the spectrum including the forest of unidentified molecular rotational features and the anomalous Galactic foreground emission in the microwave, and the diffuse interstellar bands (DIBs) and other structure in the interstellar extinction curve in the ultraviolet/visible. These astrophysical ramifications are discussed, and the dipole moments and rotational constants are tabulated to facilitate further investigations of the astrophysical role of nitrogen-substituted aromatic compounds.

Subject headings: astrochemistry — dust, extinction — infrared: ISM — ISM: lines and bands — ISM: molecules — molecular processes

1. INTRODUCTION

Most interstellar objects with associated gas and dust exhibit a series of strong infrared emission features near 3.3, 6.2, 7.7, 8.6, and 11.2 μm that are generally attributed to polycyclic aromatic hydrocarbons (PAHs) and related molecular materials (e.g., Allamandola et al. 1989, 1999 and references therein; Puget & Leger 1989; Cox & Kessler 1999). Within the framework of this PAH model, the interstellar features arise from the combined

emission of a complex mixture of PAH species that together comprise the molecular component of the carbon-rich interstellar dust population. The omnipresence and intensity of these features throughout our own Galaxy, as well as their association with many other galaxies, implies that PAHs are both common and abundant throughout the universe (Cox & Kessler 1999). Equally important, the latest observational data reveal variations in the detailed positions, profiles, and relative intensities of the interstellar emission bands—variations that correlate with object type and radiation environment (Hony et al. 2001; Peeters et al. 2002) and with spatial structure within extended objects (Sloan et al. 1997, 1999; Bregman & Temi 2005). These variations provide insight into the detailed nature of the emitting PAH population and reflect conditions within the emitting regions,

¹ Astrophysics Branch, MS 245-6, NASA Ames Research Center, Moffett Field, CA 94035.

² Corresponding author: dhudgins@mail.arc.nasa.gov.

³ Space Technology Division, MS 230-3, NASA Ames Research Center, Moffett Field, CA 94035.

giving this population enormous potential as probes of astrophysical environments.

Based on more than a decade of laboratory measurements and theoretical calculations (e.g., Hudgins et al. 2000; Vala et al. 1994; Szczepanski et al. 1995; Bauschlicher & Langhoff 1997; Kim & Saykally 2002; Mattioda et al. 2003; Oomens et al. 2003 and references therein), it is now widely recognized that models based on the composite spectra of PAHs and PAH cations can accommodate the general pattern of band positions, intensities, and profiles observed in the interstellar IR emission spectra as well as the variations in those characteristics (e.g., Langhoff 1996; Allamandola et al. 1999; Verstraete et al. 2001; Bakes et al. 2001, Draine & Li 2001; Li & Draine 2001; Pech et al. 2002). Overall, that work indicates that the interstellar 3.3 μm band and, to a lesser extent, the 11.2 μm band are dominated by the emission of *neutral* PAHs, whose most prominent bands fall in these regions. Conversely, the interstellar bands in the 6–9 μm range are dominated by the emission of *ionized* PAHs, whose most prominent bands fall in this region and are an order of magnitude more intense than those of the analogous neutral species.

Nevertheless, the agreement between the interstellar emission spectra and model spectra based on the latest experimental and theoretical data is not perfect. One issue that has emerged from the most recent analyses of the interstellar emission spectrum concerns the enigmatic position of the nominal 6.2 μm band, attributed to the CC stretching vibrations of interstellar PAH cations. Previous analyses of the IR spectra of PAH cations have shown that their dominant features in this region tend to fall at somewhat longer wavelengths than does the interstellar feature (Hudgins & Allamandola 1999, hereafter HA99). However, based on laboratory studies involving a variety of primarily small PAH cations containing 24 or fewer C atoms, HA99 noted that the position of the dominant CC stretching bands tends to shift toward shorter wavelengths with increasing molecular size and suggested that the peak position of the interstellar emission band might provide a measure of the size of the smallest members of the interstellar PAH population.

Further light was shed on the precise nature of this discrepancy by a recent observational study of more than 50 different objects based on data provided by the Short Wavelength Spectrometer (SWS) aboard the European *Infrared Space Observatory* (ISO). In that work, Peeters et al. (2002) showed that the nominal interstellar 6.2 μm band is actually a composite of two bands, one centered near 6.2 μm and one centered near 6.3 μm . Variations in the relative contributions of these two components give rise to variations in both the position and profile of the composite feature. Bands dominated by the shorter wavelength component (by far the most common case) fall at an average position of $6.215 \pm 0.021 \mu\text{m}$ (3σ range) and are designated “class A” bands. Bands that are dominated by the longer wavelength component fall at an average position of 6.295 μm and are designated “class C” bands. “Class B” bands are a composite of classes A and C and exhibit intermediate positions and compound profiles. While the data presented in HA99 do give some indication that moderately sized PAH cations ($N_C \geq 40$ C atoms) might accommodate the position of 6.3 μm class C component, the 6.2 μm component continues to defy explanation within the framework of the PAH model.

In this paper we continue our investigation into the detailed nature of the interstellar 6.2 μm PAH emission band and, in particular, the origin of the anomalous class A component of that band. In § 2, we reevaluate the possible role of the molecular size effect first noted by HA99 in light of the latest data on the spectroscopy of large PAHs (LPAHs; $N_C \geq 40$ C atoms). In § 3, the spectroscopic

properties of PAHs that incorporate one or more nitrogen atoms into their carbon skeletons (i.e., polycyclic aromatic nitrogen heterocycles or PANHs) are presented, and the potential relationship between these species and the interstellar 6.2 μm band problem is considered. Other possible factors that might influence the position of the 6.2 μm interstellar PAH emission band are treated in § 4. Finally, in § 5 several astrophysical implications of the suggestion that PANHs represent an important component of the interstellar PAH population are considered.

2. THE EFFECT OF PAH SIZE REVISITED

The issue of the discrepant positions of the nominal interstellar 6.2 μm emission band and the dominant CC stretching feature in the spectra of PAH cations has been considered previously in the literature (HA99; Peeters et al. 2002). As mentioned above, HA99 observed that the dominant CC stretching band in the spectra of PAH cations gradually shifted toward shorter wavelengths with increasing PAH size. This trend is illustrated in Figure 1a, which shows a plot of band position versus PAH size for the (purely experimental) data originally presented in HA99. Extrapolation of the observed trend led to the conclusion that its position should equal that of the interstellar band for PAHs in the 50–80 carbon atom size range. However, at the time there were few spectroscopic data available for PAH species larger than 20–30 carbon atoms by which this result could be verified. Today, as a result of a concerted effort to study larger PAH species both theoretically and in the lab, there are data by which we can test this initial suggestion.

Figure 1b shows a new version of the original position versus molecular size plot updated to include data for species that have been studied since the HA99 study. The new theoretical and experimental data are plotted as black filled circles and black filled squares, respectively, while the original HA99 data are carried over as gray filled diamonds. Also indicated on the plot are the average peak positions of the class A and C components of the nominal interstellar PAH CC stretching features. The positions of the class A and C lines have been shifted to account for the anticipated $\sim 10 \text{ cm}^{-1}$ redshift between the peak frequencies of PAH bands in absorption and emission (Cherchneff & Barker 1989; Flickinger et al. 1991; Brenner & Barker 1992; Colangeli et al. 1992; Joblin et al. 1995; Cook & Saykally 1998). Inspection of Figure 1 shows that *the general relationship between band position and PAH size observed in the smaller PAHs does not hold for the larger PAH species*. Instead, the trend seems to roll off for PAH cations larger than 30 carbon atoms with the dominant bands of these species clustering around 6.3 μm regardless of molecular size. Thus, while large PAH cations can accommodate the position of the class C interstellar band, PAH molecular size alone seems unable to explain the precise position of the class A component of the interstellar band.

3. THE EFFECT OF NITROGEN SUBSTITUTION: INTERSTELLAR PANHS

3.1. Interstellar Polycyclic Aromatic Nitrogen Heterocycles

Since molecular size alone cannot account for the position of the class A interstellar 6.2 μm emission band, we must look deeper for an explanation of the observed shift in the position of the CC stretching feature of PAH cations. In an effort to explore the origin of this and other discrepancies in detail between the interstellar emission and the spectroscopic characteristics of PAHs measured or calculated to date, we have continued to expand our studies to encompass new and different PAH-related species—species with structural or compositional characteristics that distinguish them from the other aromatic species in the database and

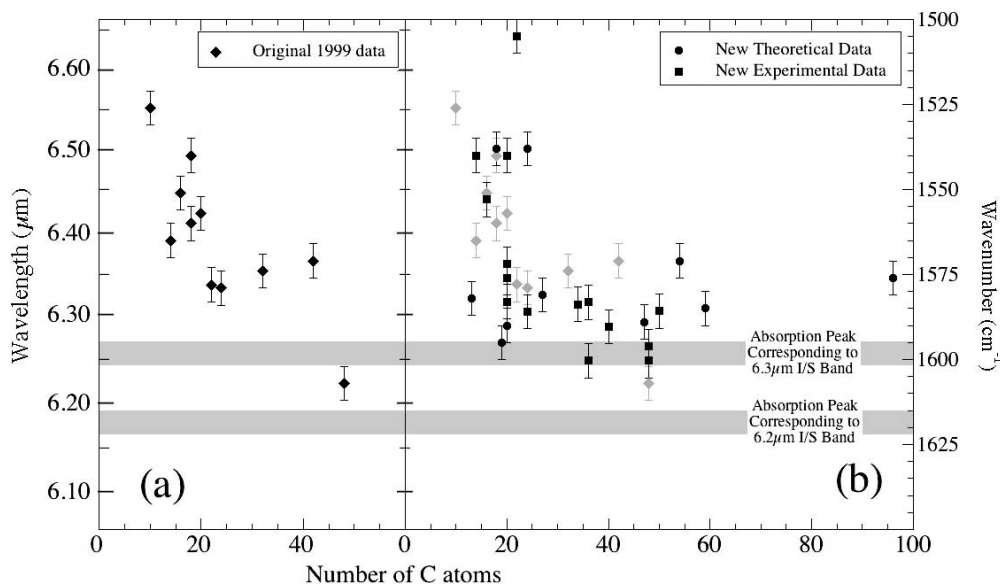


FIG. 1.—Plot of the position of the dominant CC stretching feature as a function of PAH cation size. (a) Data originally reported in HA99. (b) Same plot with data from additional species whose spectra have been measured or calculated since that time. The error bars correspond to the $\pm 5 \text{ cm}^{-1}$ (ca. $0.04 \mu\text{m}$) accuracy of matrix-isolated and calculated band positions. The shaded bars indicate the average peak positions for the interstellar class A and class C emission band components corrected for the $\sim 10 \text{ cm}^{-1}$ redshift between emission and absorption peak frequencies (see discussion in text). The error bars reflect the general accuracy of the matrix isolation. The plot demonstrates that while PAH ions composed of >30 C atoms can accommodate the class C emission component, the size effect alone is insufficient to account for the class A emission component.

that might give rise to distinctive spectroscopic properties. Among these are a series of PANHs, compounds that incorporate one or more atoms of nitrogen within their aromatic carbon skeleton. As PANHs represent a straightforward extension of the pure PAH family, and nitrogen is present in reasonable abundance in the late circumstellar envelopes in which PAHs form, PANHs might well be of significance in the astrophysical context and thus represent a natural extension of our previous experimental work.

Interstellar PAH formation is thought to occur predominantly in the circumstellar shells and outflows of carbon-rich, late-type giants (Allamandola et al. 1985, 1989; Keller 1987; Cherchneff 1996; Frenklach & Feigelson 1989). These conditions are generally modeled with the soot formation processes that occur in carbon-rich, oxygen-poor flames (Weilmunster et al. 1999). Computational studies of these processes show that growth of a PAH molecule in which one of the ring carbons has been replaced by a nitrogen can occur when a C_2H_2 feedstock molecule is replaced by an HCN molecule (Ricca et al. 2001a, 2001b). The barrier height for the HCN reaction is only slightly larger than for the all-hydrocarbon case. The studies also show that the presence of a nitrogen atom in the ring structure does not significantly affect the growth of additional, surrounding rings. Given that C_2H_2 and HCN are common and abundant species in carbon-rich circumstellar shells, it is reasonable to expect that N-substituted PAHs arise under these conditions. Furthermore, indirect support for the presence of interstellar PANHs is provided by their long-known presence in meteorites (e.g., Hayatsu et al. 1977; Hayatsu & Anders 1981; Basile et al. 1984) and the detection of several rotational lines for the simple, N-containing, three-membered ring systems 2H-azirine and aziridine along several interstellar lines of sight (Charney et al. 2001).

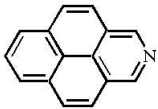
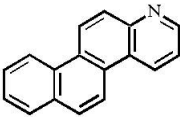
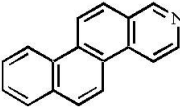
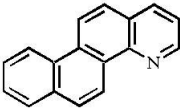
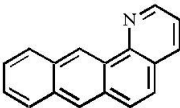
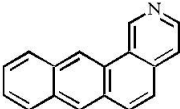
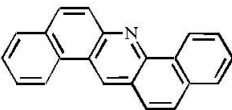
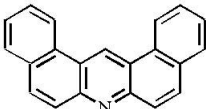
Some examples of this class of aromatic compound are given in Table 1. A detailed discussion of the general spectroscopic properties of small PANHs and PANH cations such as those shown in Table 1 can be found in the literature (Mattioda et al. 2003) and is not repeated here. Instead, we focus specifically on

the effect that nitrogen substitution has on the position of the dominant CC stretching mode near $6.2 \mu\text{m}$. Table 1 also lists the positions of the strongest bands in the $6.2 \mu\text{m}$ region for these PANH cations. Although this is not an exhaustive list of the PANH species we have studied, these results are representative of the whole. The positions of the analogous features of the corresponding pure hydrocarbon cation are also shown. Inspection of the data reveals that N substitution in these cations has only a small effect on the position of the dominant CC stretching band, and what effect there is usually tends to shift the bands toward longer, rather than shorter wavelengths. Thus, it would not appear that small PANHs can explain the observed behavior of the $6.2 \mu\text{m}$ emission band.

The species shown in Table 1 are not, however, representative of all possible PANH cations. Such an experimentally driven study is limited by the availability of starting materials; i.e., one must be able to obtain samples appropriate for study. In the case of PANHs, this constraint limited our studies to the relatively small, noncondensed species composed of 2–5 rings like those shown in Table 1. In the context of the astrophysical problem, however, much larger, condensed species are expected to dominate the interstellar PAH population (Schutte et al. 1993; Hony et al. 2001). Thus, the results of the foregoing PANH studies suffer from the same limitation as did the earliest studies of ordinary PAHs and PAH cations (i.e., pre-HA99): it is unclear to what extent the spectroscopic properties of larger, condensed members of the family can be inferred from those of the smaller, noncondensed species measured directly in the lab.

Beyond the size/structure issue, there is a second, more subtle—yet more important—characteristic of the PANH family that is not addressed in the aforementioned studies: there are two fundamentally distinct classes of PANH cations that are distinguished from one another by the position of the N substitution in the molecule. Inspection of the structures shown in Table 1 shows that for each of these species, the N atom is substituted for a CH group on the periphery of the molecule. Since the N atom

TABLE 1
EXPERIMENTALLY MEASURED POSITIONS FOR THE STRONGEST PANH CATION BANDS
IN THE 6.2 μm REGION (MATTIODA ET AL. 2003)

SPECIES	STRUCTURE	POSITION OF STRONGEST CATION BAND IN 6.2 μm REGION	
		PANH Cation (μm , cm^{-1})	Parent PAH Cation ^a (μm , cm^{-1})
2-azapyrene		6.456, 1549	6.439, 1553 ^b
1-azachrysene		6.414, 1559	6.410, 1560 ^c
2-azachrysene		6.439, 1553	6.410, 1560 ^c
4-azachrysene		6.394, 1564	6.410, 1560 ^c
1-azabenz[<i>a</i>]anthracene		6.502, 1538	6.494, 1540 ^c
2-azabenz[<i>a</i>]anthracene		6.532, 1531	6.494, 1540 ^c
Dibenz[<i>a,h</i>]acridine		6.378, 1568	6.309, 1585 ^d
Dibenz[<i>a,j</i>]acridine		6.353, 1574	6.289, 1590 ^d

^a The values for the analogous parent hydrocarbon cation are also shown for reference.

^b Hudgins & Allamandola (1995).

^c Hudgins & Allamandola (1997).

^d Unpublished experimental result.

resides on the edges of the carbon skeleton, we refer to these species as “exoskeletal” PANHs. Since an N atom is isoelectronic with a CH group, the resulting neutral species has a stable, closed-shell electronic structure (all electrons are paired), and the cations are all necessarily radical cations. This explains why the parent neutral species are sufficiently stable that we were able to obtain samples for our experimental studies.

A second, distinct class of PANHs can be formed by substituting the N atom for one of the internal C atoms in the molecular skeleton. This requires PANH structures that are larger and more

compact than those illustrated in Table 1 (see Fig. 2). Since the N atom in this class of PANH resides within the interior of the carbon skeleton, we refer to this class as “endoskeletal” PANHs. More importantly, in such a species, the substituting N atom contains one more electron than did the C atom it replaces. As a consequence, in contrast to the exoskeletal PANHs, the *neutral* endoskeletal PANHs have a radical electronic structure, while the analogous *cations* have the favorable closed-shell structure.

It is known that in flames, PAH molecules can grow by either neutral or cation intermediates with closed-shell species dominating

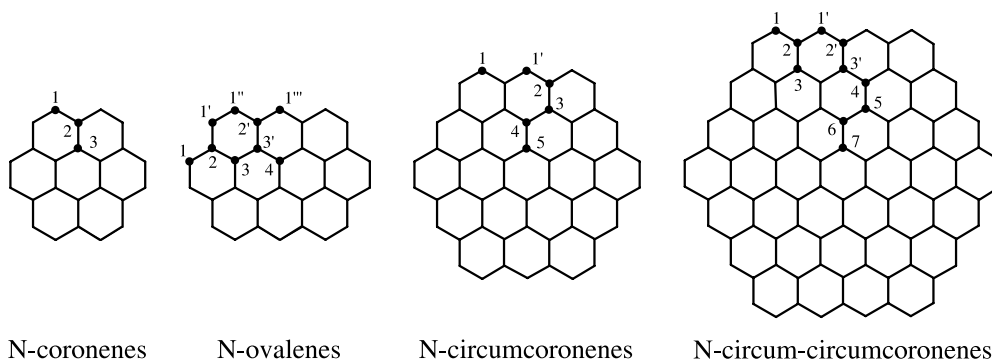


FIG. 2.—Generalized structures of the large, condensed PANH species considered in the computational component of these studies. The numbers identify the possible unique positions for N atom substitution in the structure and are assigned as described in the text.

both populations (Weilmunster et al. 1999). It is therefore reasonable to expect that an analogous cation growth mechanism involving a low level of nitrogen-containing species could yield a population of large, endoskeletal PANH cations. Thus, since an array of simple nitrogen-containing molecules including HCN and other CN-bearing carbon chain species are observed in carbon-rich late circumstellar outflows (e.g., Cernicharo et al. 1999), endoskeletal PANHs might well play a role in the astrophysical problem. Unfortunately, due to the radical nature of the precursor neutrals, such endoskeletal PANHs are not stable, and samples of such species are not available for study by our current experimental techniques. Fortunately, such exotic chemical species are accessible through modern computational methods. Indeed, such methods have already been employed to explore the potential role of closed-shell PAH (not PANH) cations in the interstellar PAH population (Hudgins et al. 2001). Consequently, in parallel to our experimental studies of PANHs, we have conducted a series of theoretical studies of the harmonic fundamental frequencies and intensities of a variety of endoskeletal PANHs. The results of those studies are discussed in § 3.2.

3.2. Endoskeletal PANHs

The computational procedures employed to explore the IR spectroscopic properties of larger, condensed PANH species have been described in detail previously (Bauschlicher & Langhoff 1997) and are summarized only briefly here. Molecular geometries are optimized, and the harmonic frequencies and infrared intensities are computed using the B3LYP (Stephens et al. 1994) hybrid (Becke 1993) functional in conjunction with the 4-31G basis sets (Frisch et al. 1984 and references therein). The harmonic frequencies are scaled by 0.958, a factor that previous work has shown brings the computed values into optimal agreement with experiment (Langhoff 1996). Previous work has also shown that the band intensities calculated in this fashion are accurate except for the neutral C–H stretches, which are overestimated by a factor of about 2 (Bauschlicher & Langhoff 1997). The C–H stretching intensity for the cations is also probably too large, but the factor is less well established. The B3LYP calculations are performed using the Gaussian98 computer codes (Frisch et al. 1998). The band positions and intensities computed in this fashion are used to generate synthetic spectra by assigning each feature a 30 cm^{-1} FWHM Gaussian profile consistent with the homogeneous line profile associated with the astrophysical emission process for the mid-IR bands.

3.2.1. Singly Substituted PANHs

The PANH species selected for our computational analyses were all N-substituted analogs of previously studied large, con-

densed PAH cations. These included all the possible substitutional isomers of the cations of coronene ($\text{C}_{24}\text{H}_{12}^+$), ovalene ($\text{C}_{32}\text{H}_{14}^+$), circumcoronene ($\text{C}_{54}\text{H}_{18}^+$), and circum-circumcoronene ($\text{C}_{96}\text{H}_{24}^+$). Generalized structures for these species are shown in Figure 2. The various isomers of these singly N-substituted species are distinguished by the following convention: a 1N prefix indicates that the N atom is substituted at the position of a CH group on the periphery of the PANH; a 2N prefix indicates substitution for a C atom one bond removed from the nearest CH group; a 3N prefix indicates substitution for a C atom two bonds removed from the nearest CH group; and so on. Two or more nonequivalent substitutions that fall into the same class are distinguished by primes added to the prefix. Under this classification scheme, all 1N-PAHs are necessarily exoskeletal PANHs, while all n N-PAHs with $n > 1$ are necessarily endoskeletal.

The first species studied were the three possible unique N-coronene cations. The structures of these species together with their calculated mid-IR spectra are shown in Figure 3, where they are also compared to the spectrum of the parent (unsubstituted) coronene cation. Note that, consistent with the designation system described above, N substitution at position 1 corresponds to replacing a CH group and yields an exoskeletal PANH, while substitution at positions 2 and 3 corresponds to replacing skeletal C atoms that are one and two bonds removed from the nearest CH group, respectively, and yield endoskeletal PANHs. Figure 3a shows the complete spectrum for each species from 2 to $50\ \mu\text{m}$. Figure 3b shows the $6\ \mu\text{m}$ region of each spectrum on an expanded scale to facilitate observing the effect of N substitution on the position of the dominant CC stretching band of each cation.

Inspection of Figure 3a shows that the PANH cations exhibit a pattern of band positions that is similar to that of the PAH cations studied to date, i.e., PANH cations do not give rise to bands in unique regions of the mid-IR not populated by the bands of the analogous pure hydrocarbon species. N substitution does, on the other hand, appear to elicit some substantial redistribution of relative band intensity, particularly with respect to the CH stretching and out-of-plane bending modes near 3.3 and $11.2\ \mu\text{m}$, respectively, both of which are substantially enhanced in the endoskeletal N-coronene cations relative to the parent coronene cation. This effect will be explored in greater detail elsewhere. Here we focus on the effect N substitution has on the position of the dominant CC stretching feature of these species.

Turning to Figure 3b, inspection of the lower two traces (the coronene and 1N-coronene cations) shows that, as was the case for the other (exoskeletal) PANH cation species studied experimentally and discussed in § 3.1, substitution at the 1 position has little effect on the position of the dominant band in the $6.2\ \mu\text{m}$ region (6.452 vs. $6.441\ \mu\text{m}$ in unsubstituted coronene). On the

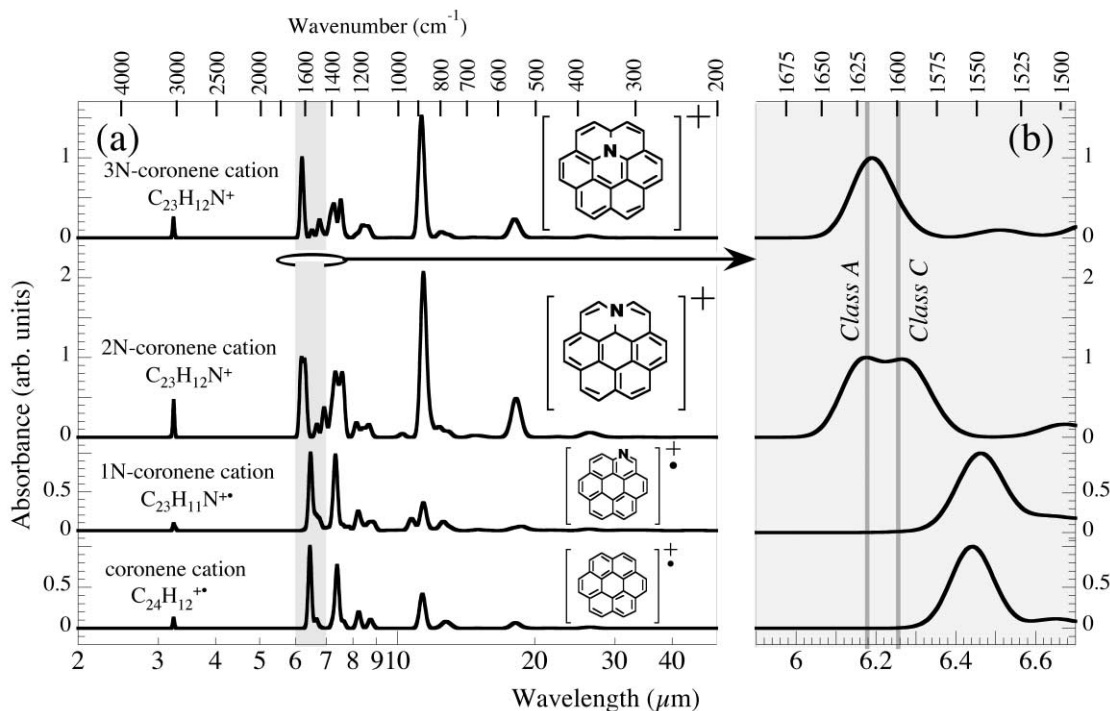


FIG. 3.—Calculated IR spectra of the three possible N-substituted coronene cations compared to that of the parent (unsubstituted) hydrocarbon. (a) Complete spectrum from 2 to 50 μm . (b) Blowup of the 6 μm region of each spectrum. The average positions of the interstellar class A and class C 6.2 μm emission components (Peeters et al. 2002) are indicated in (b), shifted to compensate for the $\sim 10\text{ cm}^{-1}$ redshift difference between emission and absorption peak frequencies (§ 2). Note that the coronene cation and the exoskeletal 1N-coronene cation have radical electronic structures (denoted with a dot), while the endoskeletal 2N- and 3N-coronene cations have the more favorable closed-shell structures. All spectra are normalized to the intensity of the strongest band in the 6.2 μm region.

other hand, the results for the endoskeletal positions, shown in the top two traces of Figure 3, are more intriguing. The figure shows that the dominant feature in the 6.2 μm region for both the 2N- and 3N-coronene cations undergoes a significant blueshift, falling at exactly the position of the interstellar class A 6.2 μm emission component (indicated by a vertical bar). This effect is quantified in Table 2, which gives the molecular characteristics and positions of the dominant CC stretching features in the 6.2 μm region for each of the N-coronene cations compared to that of the parent coronene cation. Inspection of those data reveals that for the endoskeletal N substitution positions, the dominant band in this region is shifted to 6.177 and 6.184 μm for substitution at positions 2 and 3, respectively.

It is also worth noting that this effect is ionization dependant. Calculations on the analogous neutral N-coronenes have shown that the spectroscopic effect of N substitution on the position of the dominant CC stretching feature—whether exoskeletal or endoskeletal—is neither as large nor as consistent as it is in the cations. These data are tabulated in the second section of Table 2. Indeed, inspection of the salient data reveals that, if anything, N substitution in the neutral species tends to produce a *redshift* from the position of the band in the parent neutral coronene and fails to reproduce the position of the class A interstellar band.

An inspection of Table 2 shows that the open-shell exoskeletal 1N-coronene cation has a much smaller shift in the band position than the endoskeletal cations. Adding an H atom to the 1N-coronene cation yields the closed-shell species denoted 1NH-coronene $^+$ in Table 2. The dominant band of the 1NH-coronene cation is at 6.254 μm , which is more consistent with the values found for the closed-shell 2N- and 3N-coronene cations. Since the closed-shell endoskeletal systems are much less computationally demanding and should represent an upper bound to the

shift for the open-shell systems, we consider the closed-shell 1NH- species for the remainder of this manuscript. As we show below, the closed-shell exoskeletal systems are not critical for understanding the 6.2 μm feature, and therefore we conclude that the open-shell exoskeletal systems do not contribute to the 6.2 μm feature either. For simplicity, from this point on we drop the H and denote the closed-shell exoskeletal systems as “1N-.”

To see whether the foregoing result was an anomaly or a general spectroscopic property of endoskeletal PANH cations, our computational studies were extended to include the N-substituted analogs of the ovalene, circumcoronene, and circum-circumcoronene cations. As was the case for the N-coronenes (Fig. 3a), the global distribution of band positions and intensities across the spectrum of these larger cations is entirely consistent with that of other large aromatic cations. Thus, we focus here specifically on the characteristics of the feature(s) in the 6 μm region. The results for the N-ovalene and N-circumcoronene cations are plotted in Figure 4, with the substitutional position corresponding to each trace labeled according to the designations given in Figure 2. The spectral representations of the data for the N-ovalene cations are plotted as a function of depth into the molecular skeleton in Figure 4a. Likewise, Figure 4b shows the analogous progression for the N-circumcoronenes. For reference, the features are compared to those of the analogous parent PAH cation and the canonical class A (*top trace*) and class C (*bottom trace*) interstellar emission bands identified by Peeters et al. (2002). The positions and shifts of the dominant feature in the 6.2 μm region for all of these species are tabulated in Table 2. Consistent with the results for the N-coronenes, the position of the dominant CC stretching band is observed to shift steadily to shorter wavelengths as the depth of the N substitution into the C skeleton of the molecule increases. This trend is quantified for all these species in the plot shown in Figure 5.

TABLE 2
MOLECULAR CHARACTERISTICS AND COMPUTED POSITIONS OF THE DOMINANT 6.2 μm BANDS FOR A RANGE
OF SINGLY SUBSTITUTED PANHS COMPARED TO THEIR PARENT HYDROCARBONS

SPECIES	FORMULA	EXO-/ENDOSKELETAL N	C/N RATIO	DOMINANT 6.2 μm CC STRETCHING BAND POSITION			
				λ (μm)	$\Delta\lambda$ (μm)	$\tilde{\nu}$ (cm^{-1})	$\Delta\tilde{\nu}$ (cm^{-1})
Coronene cation.....	$\text{C}_{24}\text{H}_{12}^+$	6.441	...	1553	...
1N-coronene ⁺	$\text{C}_{23}\text{H}_{11}\text{N}^+$	Exo	23	6.452	+0.011	1550	-3
1NH-coronene ⁺	$\text{C}_{23}\text{H}_{12}\text{N}^+$	Exo	23	6.254	-0.187	1599	+35
2N-coronene ⁺	$\text{C}_{23}\text{H}_{12}\text{N}^+$	Endo	23	6.177 ^a	-0.222	1619 ^a	+55
3N-coronene ⁺	$\text{C}_{23}\text{H}_{12}\text{N}^+$	Endo	23	6.184	-0.257	1617	+64
Coronene neutral.....	$\text{C}_{24}\text{H}_{12}$	6.240	...	1603	...
1N-coronene.....	$\text{C}_{23}\text{H}_{11}\text{N}$	Exo	23	6.268	+0.028	1596	-7
2N-coronene.....	$\text{C}_{23}\text{H}_{12}\text{N}$	Endo	23	6.317	+0.077	1583	-20
3N-coronene.....	$\text{C}_{23}\text{H}_{12}\text{N}$	Endo	23	6.219	-0.021	1608	+5
Ovalene cation.....	$\text{C}_{32}\text{H}_{14}^+$	6.415	...	1559	...
1N-ovalene ^{+b}	$\text{C}_{31}\text{H}_{14}\text{N}^+$	Exo	31	6.320	-0.095	1582	+23
1'N-ovalene ^{+b}	$\text{C}_{31}\text{H}_{14}\text{N}^+$	Exo	31	6.332	-0.083	1579	+20
1''N-ovalene ^{+b}	$\text{C}_{31}\text{H}_{14}\text{N}^+$	Exo	31	6.324	-0.091	1581	+22
1'''N-ovalene ^{+b}	$\text{C}_{31}\text{H}_{14}\text{N}^+$	Exo	31	6.268	-0.147	1595	+36
2N-ovalene ⁺	$\text{C}_{31}\text{H}_{14}\text{N}^+$	Endo	31	6.267	-0.148	1596	+37
2'N-ovalene ⁺	$\text{C}_{31}\text{H}_{14}\text{N}^+$	Endo	31	6.277	-0.138	1593	+34
3N-ovalene ⁺	$\text{C}_{31}\text{H}_{14}\text{N}^+$	Endo	31	6.243	-0.172	1602	+43
3'N-ovalene ⁺	$\text{C}_{31}\text{H}_{14}\text{N}^+$	Endo	31	6.231	-0.184	1605	+46
4N-ovalene ⁺	$\text{C}_{31}\text{H}_{14}\text{N}^+$	Endo	31	6.202	-0.213	1612	+53
Circumcoronene cation.....	$\text{C}_{54}\text{H}_{18}^+$	6.365	...	1571	...
1N-circumcoronene ^{+b}	$\text{C}_{53}\text{H}_{18}\text{N}^+$	Exo	53	6.252 ^c	-0.113	1600 ^c	+29
1'N-circumcoronene ^{+b}	$\text{C}_{53}\text{H}_{18}\text{N}^+$	Exo	53	6.309	-0.056	1585	+14
2N-circumcoronene ⁺	$\text{C}_{53}\text{H}_{18}\text{N}^+$	Endo	53	6.250	-0.115	1600	+29
3N-circumcoronene ⁺	$\text{C}_{53}\text{H}_{18}\text{N}^+$	Endo	53	6.234	-0.131	1604	+33
4N-circumcoronene ⁺	$\text{C}_{53}\text{H}_{18}\text{N}^+$	Endo	53	6.215	-0.150	1609	+38
5N-circumcoronene ⁺	$\text{C}_{53}\text{H}_{18}\text{N}^+$	Endo	53	6.211	-0.154	1610	+39
Circum-circumcoronene cation.....	$\text{C}_{96}\text{H}_{24}^+$	6.345	...	1576	...
2N-circumcircumcor ⁺	$\text{C}_{95}\text{H}_{24}\text{N}^+$	Endo	95	6.262	-0.083	1597	+21
2'N-circumcircumcor ⁺	$\text{C}_{95}\text{H}_{24}\text{N}^+$	Endo	95	6.266	-0.079	1596	+20
3N-circumcircumcor ⁺	$\text{C}_{95}\text{H}_{24}\text{N}^+$	Endo	95	6.305	-0.040	1586	+10
3'N-circumcircumcor ⁺	$\text{C}_{95}\text{H}_{24}\text{N}^+$	Endo	95	6.281	-0.064	1592	+16
4N-circumcircumcor ⁺	$\text{C}_{95}\text{H}_{24}\text{N}^+$	Endo	95	6.277	-0.068	1593	+17
5N-circumcircumcor ⁺	$\text{C}_{95}\text{H}_{24}\text{N}^+$	Endo	95	6.256	-0.089	1599	+23
6N-circumcircumcor ⁺	$\text{C}_{95}\text{H}_{24}\text{N}^+$	Endo	95	6.258	-0.087	1598	+22
7N-circumcircumcor ⁺	$\text{C}_{95}\text{H}_{24}\text{N}^+$	Endo	95	6.242	-0.103	1602	+26

^a Shorter wavelength component of a doublet; a longer wavelength component with similar intensity falls at a position of 6.274 μm (1594 cm^{-1}).

^b Closed-shell, protonated form of the exoskeletal PANH cation. See discussion in text (§ 3.2.1).

^c Shorter wavelength component of a doublet; a longer wavelength component with similar intensity falls at a position of 6.452 μm (1550 cm^{-1}).

A subsequent analysis of the computational output has revealed that the presence of the N atom in an endoskeletal position within these cations produces a modest but significant redistribution of the electron density within the molecule. This redistribution produces two changes: (1) subtle changes in the CC bond force constants within the carbon skeleton of the cation and (2) changes in the dipole derivatives. These two changes result in a blueshift of the dominant band in the region from 6.3 to 6.2 μm . This effect is perhaps not surprising in view of nitrogen's high "electronegativity," a measure of an atom's relative attraction for the electrons it shares with another atom in a chemical bond. In summary, while the global character of the spectra of PANHS is consistent with that of the analogous PAH species, important differences in detail are observed in the bands falling in the 1550–1650 cm^{-1} (6.45–6.06 μm) region of the spectrum. As demonstrated by Figure 5, the position of the CC stretching feature in endoskeletal PANH cations can accommodate the position of the class A interstellar emission component.

Careful inspection of the data in Table 2 shows that the shortest wavelength feature achieved in the N-coronenes falls at

$\lambda_{\text{min}} = 6.184 \mu\text{m}$ ($\tilde{\nu}_{\text{min}} = 1617 \text{cm}^{-1}$), 0.257 μm shorter in wavelength (64 cm^{-1} higher in frequency) than the corresponding feature in the unsubstituted coronene cation. However, the minimum wavelength and maximum blueshift achieved by the N-ovalenes are 6.202 and 0.213 μm (1612 and 53 cm^{-1}), respectively, while those of the N-circumcoronenes and N-circum-circumcoronenes are only 6.211 and 0.154 μm (1610 and 39 cm^{-1}) and 6.242 and 0.103 μm (1602 and 26 cm^{-1}), respectively. Thus, we see that the magnitude of the blueshift decreases with increasing molecular size. Since this blueshift provides a measure of the extent by which the N atom perturbs the electron density in the molecule, we conclude that the influence of the N atom, its ability to alter the distribution of electron density across the molecule, is diluted as the size of the carbon skeleton increases.

3.2.2. Multiply Substituted PANHS

Given the potential astrophysical significance of endoskeletal PANH cations implied by the foregoing analysis of singly N-substituted species and the observation that the shift decreases

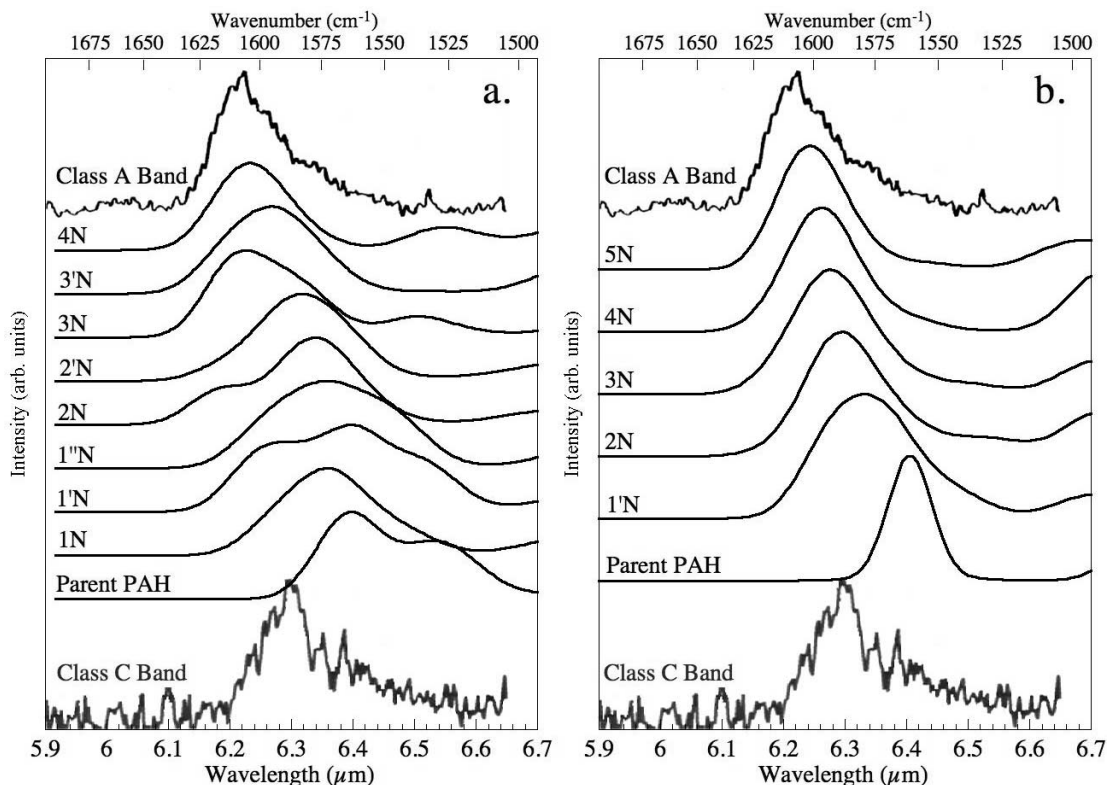


FIG. 4.—Calculated IR spectra of the possible N-substituted cations of (a) ovalene and (b) circumcoronene in the $6 \mu\text{m}$ region. The substitutional position of each corresponds to the designations given with the structures in Fig. 2. The features of the various PANH cations are compared to those of the unsubstituted PAH cation and the “pure” class A and class C emission bands identified by Peeters et al. (2002). The calculated bands have been redshifted by 10 cm^{-1} to compensate for the expected difference between emission and absorption peak frequencies (§ 2). All spectra are normalized to the intensity of the strongest band in the $6.2 \mu\text{m}$ region.

for a single nitrogen atom with increasing numbers of carbon atoms, it is a natural extension of this work to explore how PANHs bearing more than one N atom might contribute to the astrophysical problem. However, due to the exponentially growing number of possible isomers, as well as a number of chemical issues related to the growth and charge state of multiply N-substituted PANHs, such an analysis rapidly becomes extremely complex. Consequently, an exhaustive analysis of the chemical characteristics

and spectroscopy of multiply N-substituted PANHs is beyond the scope of this paper, and we have therefore limited our studies to those doubly and triply substituted PANH cations that are likely to exhibit the most pronounced spectroscopic effects. Here we briefly summarize the key implications of that work.

As noted above for a single nitrogen atom, the magnitude of the blueshift decreases with increasing molecular size. To explore this dilution effect, we have expanded our study to include selected doubly endoskeletal-substituted cations of N-circumcoronene and N-circum-circumcoronene and one triply endoskeletal-substituted N-circumcoronene cation. While substitution by more than one N atom can enhance the spectroscopic impacts discussed in § 3.2.1, it does not give rise to any additional, distinctive spectral features that fall outside the envelope encompassed by normal PAH features. Indeed, even in the unlikely event that two nitrogen atoms were substituted adjacent to one another within the carbon skeleton, the resulting aromatic NN stretching motion mixes effectively with the CC stretching and CH in-plane bending modes of the molecule, and the resulting features fall within the envelope of the interstellar $7.6/7.8/8.6 \mu\text{m}$ emission complex.

The inclusion of additional N atoms within the structures of the larger species can overcome the dilution effect noted above. For example, the addition of a second endoskeletal N atom within the structure of an N-circumcoronene cation further blueshifts the dominant feature in this region as far as $6.177 \mu\text{m}$ (1619 cm^{-1}), very close to the position achieved by the singly substituted N-coronenes. Thus, for a molecule the size of circumcoronene ($N_C \sim 50 \text{ C atoms}$) the combined influence of two endoskeletal N atoms is required to produce the same effect that a single N atom produces in the smaller N-coronene cation. Even larger species would require a commensurately larger number of N atoms to

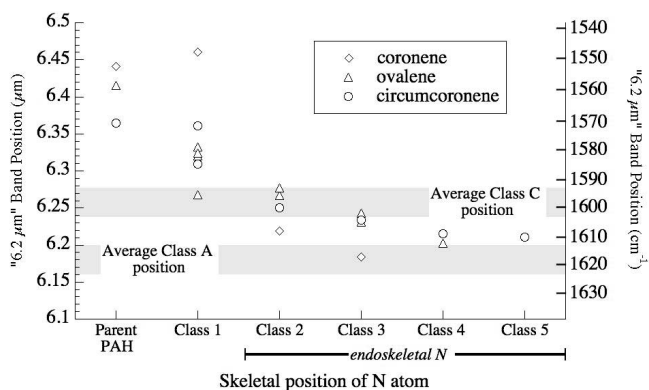


FIG. 5.—Position of the dominant CC stretching band for N-coronene, N-ovalene, and N-circumcoronene as a function of the positional class of the N substitution. The structures of the species considered are shown in Fig. 2 with the various unique positions for N atom substitution indicated and numbered as described in the text. The average positions of the interstellar class A and class C $6.2 \mu\text{m}$ emission components (Peeters et al. 2002) are indicated but shifted to compensate for the $\sim 10 \text{ cm}^{-1}$ redshift difference between emission and absorption peak frequencies (§ 2).

maintain the full measure of the N-associated blueshift. For the circum-circumcoronene, two multiply substituted species were studied; the species with two endoskeletal 7N atoms showed a shift to $6.229 \mu\text{m}$ (1606 cm^{-1}), while the three endoskeletal 7N nitrogen atoms showed a marginally larger shift to $6.225 \mu\text{m}$ (1607 cm^{-1}).

Finally, it is important to note that the blueshifting of the dominant $6.2 \mu\text{m}$ CC stretching feature that accompanies endoskeletal N substitution does not continue ad infinitum. Rather, this effect reaches a limit around $6.18 \mu\text{m}$. N substitution beyond that required to shift the dominant CC stretching feature to that limit has little or no effect on the band position. The reason for this behavior is straightforward. As discussed above, there is an asymmetry in the electron distribution between the interior and the edges of large, unsubstituted PAH cations, and the presence of an electronegative N atom (or atoms) within the C skeleton tends to smooth out this asymmetry, thereby shifting the associated CC stretching vibrations to shorter wavelengths. However, once the electron distribution is essentially uniform over the carbon skeleton, the impact of the N is essentially washed out, and the inclusion of additional N atoms has no further effect on the band position.

While far from complete, our tests using multiply substituted PANHs support the view that as the number of carbon atoms increases, more nitrogen atoms are required to produce the same shift. The important astrophysical implications of this effect are discussed in § 5 below.

4. OTHER POSSIBLE SPECTROSCOPIC INFLUENCES

The results presented in § 3 provide a strong case that N substitution in interstellar PAHs can explain the position of the class A interstellar $6.2 \mu\text{m}$ emission component. This does not, however, establish that there are not other, equally feasible origins for this anomalous feature. For example, aside from altering the electron density distribution in the molecule, substitution of one or more N atoms into the structure of a PAH lowers the symmetry of the molecule. The lower a molecule's symmetry, the greater the fraction of its vibrational modes that are IR active. This raises the question of whether it might be the lower molecular symmetry rather than nitrogen's inherent electronegativity that activates the crucial shorter wavelength CC stretching modes that underlie the interstellar class A $6.2 \mu\text{m}$ emission component. On the other hand, if the influence of a heteroatom (an atom other than carbon or hydrogen) is necessary to produce the band shift, is the effect unique to nitrogen, or would any heteroatom be sufficient to produce the shift? Finally, multiple ionization would be expected to change the electron density distribution in the molecule; might it also affect the position of the dominant CC stretching band(s)? To answer these questions, we have carried out additional calculations to determine the influence of symmetry, substitution by heteroatoms other than N, and multiple ionization on PAH features in the $6.2 \mu\text{m}$ region. The results of these studies are summarized in Table 3 and discussed in the following sections. For reference, the corresponding information for the parent coronene, ovalene, and circumcoronene cations is also included at the top of the table.

4.1. *The Effect of Symmetry Lowering on the Spectrum*

The calculations for the unsubstituted coronene cation show that while the dominant CC stretching mode falls at $6.439 \mu\text{m}$ (1553 cm^{-1}), the molecule has other weak or IR-inactive vibrations that fall at wavelengths as short as $6.238 \mu\text{m}$ (1603 cm^{-1}). The circumcoronene cation also has similar IR-inactive modes that fall shortward of its dominant CC stretching band ($6.365 \mu\text{m}$, 1571 cm^{-1}). N substitution, therefore, does not give rise to new vibrational modes per se, but rather shifts the CC stretching

bands to slightly shorter wavelengths and “lights up” modes at shorter wavelengths that are weak or inactive in the parent PAH cation. To determine whether this redistribution of intensity is a symmetry effect or whether it depends on the presence of a heteroatom in the structure, we computed the spectra of three PAH cations similar in size to the circumcoronene cation, but whose symmetries have been altered by modifications to the ring structure rather than substitution of a heteroatom. The structures of the species studied are shown together with the position of their dominant feature in the $6.2 \mu\text{m}$ region in rows A, B, and C of Table 3. The structures of rows A and B represent species that are derived by removing one and two rings from circumcoronene, respectively. The structure in row C is a species of approximately the same size as circumcoronene, but with a different, lower symmetry structure.

Not surprisingly, the general patterns of band positions and intensities across the $2.5\text{--}25 \mu\text{m}$ spectra of these PAH cations are similar to one another and are entirely consistent with those of other PAH cations. The complete spectroscopic data will be reported and discussed in a future publication. Here, we focus on the position of the dominant CC stretching feature in the $6.2 \mu\text{m}$ region and the influence, if any, that molecular symmetry has on that position. Comparison of the data in rows A–C of Table 3 shows that while lowering the symmetry does cause some minor blueshifting of the dominant feature in this region, the magnitude of this effect is substantially smaller than is required to accommodate the class A interstellar $6.2 \mu\text{m}$ emission component. A detailed analysis of the computational data reveals that while the change in molecular symmetry modestly perturbs the fundamental frequencies of the IR-active modes, it produces little or no intensity transfer to the pivotal inactive modes lying shortward of those modes. Thus, we conclude that lowered symmetry alone is insufficient to account for the band shifts observed in the endoskeletal PANH cations.

4.2. *The Effect of Heteroatoms Other Than Nitrogen on the Spectrum*



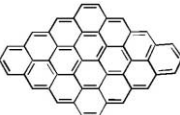




The foregoing results imply that the influence of a heteroatom is critical to activating the CC stretching modes that underlie the class A $6.2 \mu\text{m}$ interstellar emission component. While, as discussed in § 5 below, cosmic abundances significantly constrain the inventory of potential heteroatom substituents, N is by no means the only possible candidate. Of the other heteroatomic species, silicon (Si) and oxygen (O) are particularly attractive—the former because of its identical valence electron structure (and therefore similar chemical characteristics) to carbon, and the latter because of its relative cosmic abundance and high electronegativity (i.e., electron-withdrawing nature).

Although silicon is less abundant than carbon ($[\text{Si}]/[\text{C}] \sim 0.1$), we explored its effects on the IR spectrum of PAHs because that element plays an important chemical role in many circumstellar PAH formation zones. In addition, since its valence electron structure is identical to that of carbon, it can substitute easily (from a bonding standpoint) anywhere within the carbon skeleton of a PAH. Unlike N, however, the electronegativity of Si is relatively low. Indeed, it is even less than that of C. Thus, these species provide insight into whether the disruption of any heteroatom within the PAH structure is sufficient to produce the band blueshift observed in the endoskeletal N compounds or whether the electron-withdrawing nature of the heteroatom is crucial to the effect.

The results of these computations are summarized in rows D and E of Table 3, which show the positions of the dominant CC stretching feature corresponding to the endoskeletal silicon-substituted cations 4Si-ovalene and 5Si-circumcoronene (based

TABLE 3

A SUMMARY OF THE EFFECTS OF VARIATIONS IN PAH STRUCTURE AND COMPOSITION ON THE POSITION OF THE DOMINANT CC STRETCHING FEATURE

ROW LABEL	SPECIES	FORMULA	STRUCTURE	DOMINANT 6.2 μm CC STRETCHING BAND POSITION	
				λ (μm)	$\tilde{\nu}$ (cm^{-1})
Reference	Coronene cation	$\text{C}_{24}\text{H}_{12}^+$	see Fig. 2	6.441	1553
Reference	Ovalene cation	$\text{C}_{32}\text{H}_{14}^+$	see Fig. 2	6.415	1559
Reference	Circumcoronene cation	$\text{C}_{54}\text{H}_{18}^+$	see Fig. 2	6.365	1571
Lowered Symmetry Effects					
A.....	Circumcoronene cation – 1 ring	$\text{C}_{52}\text{H}_{18}^+$		6.357	1573
B.....	Circumcoronene cation – 2 rings	$\text{C}_{50}\text{H}_{18}^+$		6.344	1576
C.....	Circumpyrene cation	$\text{C}_{48}\text{H}_{18}^+$		6.317	1583
Heteroatom Effects					
D.....	4Si-ovalene cation	$\text{C}_{31}\text{H}_{14}\text{Si}^+$		6.439	1553
E.....	5Si-circumcoronene cation	$\text{C}_{53}\text{H}_{18}\text{Si}^+$		6.382	1567
F.....	1O-circumcoronene cation	$\text{C}_{53}\text{H}_{17}\text{O}^+$		6.321	1582
G.....	1'O-circumcoronene cation	$\text{C}_{53}\text{H}_{17}\text{O}^+$		6.281	1592
H.....	Coronene-iron cation complex	$\text{C}_{24}\text{H}_{12}\cdots\text{Fe}^+$	$\text{cor}\cdots\text{Fe}^+$	6.277	1593
I.....	Coronene-magnesium cation complex	$\text{C}_{24}\text{H}_{12}\cdots\text{Mg}^+$	$\text{cor}\cdots\text{Mg}^+$	6.270	1595
J.....	Coronene-magnesium dication complex	$\text{C}_{24}\text{H}_{12}\cdots\text{Mg}^{2+}$	$\text{cor}\cdots\text{Mg}^{2+}$	6.317	1583 ^a
Multiple Ionization Effects					
K.....	Coronene ^{2+b}	$\text{C}_{24}\text{H}_{12}^{2+}$	see Fig. 2	6.423	1557
L.....	Ovalene ^{2+b}	$\text{C}_{32}\text{H}_{14}^{2+}$	see Fig. 2	6.394	1564
M.....	Circumcoronene ^{2+b}	$\text{C}_{54}\text{H}_{18}^{2+}$	see Fig. 2	6.361	1572
N.....	Circumcoronene ^{3+b}	$\text{C}_{54}\text{H}_{18}^{3+}$	see Fig. 2	6.433	1554

^a The results for the singlet state; the triplet, which is only marginally higher in energy, yields 1543 cm^{-1} .^b Data from Bauschlicher & Bakes (2000).

on the designation scheme employed in § 3 to distinguish the various N-substituted compounds). Note that these species are the silicon analogs of two of the N-substituted species that gave the largest blueshifts. It should be noted that although Si can accommodate the same bonding as C, a Si atom has a significantly larger atomic radius than does a C atom. Consequently, the Si—C bonds in these structures are longer than C—C bonds, resulting in a sizable distortion of the rings containing the Si and distorting the planarity of the structure in this region. Nevertheless, the overall spectroscopic characteristics of these species are similar to those of the parent PAH cation. However, unlike the N substitution case, inspection of Table 3 shows that Si substitution results in a small redshift of the CC stretching frequency compared to the parent cation. Thus, it would appear that a strongly electron-withdrawing nature is crucial to producing a blueshift in the position of the dominant CC stretching feature. In view of this and the chemical effect of ring distortion, we conclude that it is unlikely that Si substitution plays an important role in understanding the position of the interstellar CC stretching band.

Oxygen, on the other hand, is highly electron withdrawing—indeed, even more so than is nitrogen. In addition, its cosmic abundance is approximately a factor of 5 greater than that of nitrogen. Thus, in view of what we have learned from the studies presented up to this point, O substitution would appear to present an attractive possible alternative to N substitution for inducing a similar blueshift to the CC stretch. However, oxygen's valency requirements place severe restrictions on the possible positions an O heteroatom can occupy within the structure of a PAH cation. In particular, unlike N, an O atom substituted into a PAH cation cannot bond to three adjacent, internal C atoms without sacrificing the aromatic stabilization about that point in the network. Effectively, this limits oxygen substitution to the outer edges of the peripheral rings and precludes endoskeletal substitution—a critical aspect of band shifting found in PANH cations. Nevertheless, to determine the effect of O substitution for carbon at a peripheral position, we calculated the spectra of the 10- and 1'O-circumcoronene cations, the two possible exoskeletal O-substituted variants. The structures of these species are shown in rows F and G of Table 3 together with the positions of their dominant CC stretching features. While the 10–20 cm^{-1} shift in these bands from the position of the unsubstituted parent cation is somewhat greater than that found for the other variants considered in this phase of the study, it is still much smaller than the nearly 50 cm^{-1} blueshift required to accommodate the position of the interstellar class A 6.2 μm emission feature. Thus, although oxygen is, in principle, sufficiently electron withdrawing to redistribute the electron density toward the interior of the carbon skeleton, the more limited valency of the oxygen atom prevents it from occupying a position in the structure where it can fully manifest this effect.

4.3. The Effect of Metal Complexation on the Spectrum

Another class of heteroatomic PAH-related species that might, in principle, play a role in the astrophysical problem are metallocenes—the generic name given to complexes that form between aromatic compounds and the atoms of many metals. These are very stable species in which a metal atom resides either above or below the plane of the molecule, not substituted within the ring network. For transition metal atoms, this can be more than just simple electrostatic attraction; in such complexes, the occupied metal *d* orbitals can donate charge to the PAH unfilled π^* orbitals, and the occupied PAH π orbitals can donate charge into empty or partly occupied metal orbitals to produce a strong, pseudocovalent bond. These compounds have begun to attract increasing interest in recent years in fields such as physical and

organometallic chemistry for their interesting and unique bonding characteristics (see, e.g., Buchanan et al. 1998; Senapati et al. 2003). Given the relative cosmic abundance of the metals iron and magnesium, complexes involving these metals or their ions might well be important in the astrophysical context (Serra et al. 1992; Klotz et al. 1995).

To explore the spectroscopic properties of this class of species, we have undertaken calculations of the complexes of the PAH coronene ($\text{C}_{24}\text{H}_{12}$) with the metal ions Fe^+ , Mg^+ , and Mg^{2+} in their quartet, doublet, and singlet spin states, respectively. Interestingly, the lowest energy structures for these complexes have the metal ion positioned over one of the peripheral rings of the coronene structure, rather than the central ring. Those calculations indicate that the global pattern of band positions and intensities in the IR spectra of these metallocene complexes are more reminiscent of the spectrum of neutral coronene than they are of the spectrum of the coronene cation, particularly for the singly charged $\text{C}_{24}\text{H}_{12} \cdots \text{Fe}^+$ and $\text{C}_{24}\text{H}_{12} \cdots \text{Mg}^+$ complexes. This finding is consistent with charge on these complexes residing primarily on the metal atom—an interesting result in view of the fact that the ionization potentials (IPs) of the species involved (Mg , $\text{IP}_1 = 7.6$ eV, $\text{IP}_2 = 15.0$ eV; Fe , $\text{IP}_1 = 7.9$ eV) are all similar to or greater than that of coronene (7.3 eV; Jochims et al. 1999). Despite the smaller coronene IP, the $\text{C}_{24}\text{H}_{12} \cdots \text{M}^+$ is more stable because the bonding is stronger in $\text{C}_{24}\text{H}_{12} \cdots \text{M}^+$ than in the $\text{C}_{24}\text{H}_{12}^+ \cdots \text{M}$. Again, the complete spectra of these species will be treated in detail in a future publication, while we focus here on the 6.2 μm region of the spectrum.

Inspection of rows H, I, and J in Table 3 shows that the dominant 6.2 μm features of the three metallocene ion complexes (ranging from 6.27 to 6.32 μm) are significantly blueshifted from the position of the bare coronene cation (6.439 μm). However, care must be exercised in interpreting this result. As mentioned above, the general spectroscopic character of these species is more akin to that of the neutral coronene molecule, and the dominant feature of that species in this region falls at 6.238 μm —itself even shorter in wavelength than the metallocene ion complexes. The positions of the dominant 6.2 μm coronene bands in the metallocene ion complexes are, therefore, intermediate between the positions of the dominant bands in bare neutral and cationic coronene, presumably reflecting a partially charged character induced by the adjacent metal cation. Thus, it is likely that the position of the metallocene band reflects the intermediate ionization state induced by the adjacent metal cation rather than the activation of short-wavelength modes in the molecule. In any event, these results provide no indication that complexation of a PAH has the capacity to shift its dominant CC stretching feature in the 6.2 μm region outside of the region bounded by the analogous bands of the bare neutral and cationic parent PAH. Since the extensive studies of the IR spectra of neutral and ionized PAHs available in the literature have established that these latter species cannot accommodate the position of the class A interstellar emission band, it is unlikely that metallocene complexes will do so either. Although this work should not be viewed as an exhaustive exploration of the spectroscopic properties of metallocene complexes and their potential astrophysical importance, it does not appear that such species are likely to provide an explanation for this aspect of the astrophysical problem.

4.4. The Effect of Multiple Ionization on the Spectrum

One final possible alternative source for the anomalous position of the interstellar class A 6.2 μm emission component that we consider here is multiple ionization. To date, experimental

studies of the IR spectra of ionized PAHs have been limited to singly charged species, although astrophysical models indicate that multiply charged species may play an important role in the most energetic emission zones (Bakes et al. 2001). However, theoretical spectroscopic studies of such species conducted using techniques similar to those employed in the current study have been reported previously (Bauschlicher & Bakes 2000). As the effect of multiple ionization on the position of the dominant 6.2 μm feature was not explicitly examined by Peeters et al. (2002), we revisit those earlier results here.

The positions of the dominant CC stretching features for the multiply charged PAH cations calculated and presented graphically by Bauschlicher & Bakes (2000) are tabulated in rows K–N of Table 3. The species considered include the dications of coronene and ovalene and both the di- and trications of circumcoronene. Comparison of the band positions for each of these species to that of the corresponding singly charged ion reveals that multiple ionization has little, if any, consistent effect on the position of the dominant PAH bands in the 6.2 μm region. Thus, once again, it would not appear that this factor can account for the short-wavelength component of the interstellar 6.2 μm emission band.

In summary, the computational studies reported here indicate that nitrogen substitution in the interior rings of a PAH cation produces a blueshift in the position of the dominant CC stretching vibration that is sufficient to account for the position of the class A component of the interstellar 6.2 μm emission band. On the other hand, these studies indicate that analogous substitution by silicon atoms, peripheral substitution by oxygen atoms, complexation with metal atoms, and lowering the molecular symmetry do not appear to exhibit a similar ability to accommodate the precise position of the interstellar feature. Previously reported calculations show that multiple ionization also fails in this regard. Thus, we conclude that interstellar PAHs containing nitrogen are the best candidates to match the 6.22–6.30 μm range observed for the CC stretching band by Peeters et al. (2002).

5. ASTROPHYSICAL IMPLICATIONS

5.1. A Phenomenological Review of the Case for PANHs

As discussed in § 4, endoskeletal PANH cations are the only species studied to date in our combined experimental and theoretical studies that can accommodate a strong emission feature at the 6.215 μm position of the class A PAH emission component. However, aside from these spectroscopic studies, one can make a sound circumstantial argument that nitrogen-substituted aromatic compounds represent the best candidates for explaining the anomalous interstellar feature. We can understand this argument by examining the constraints that the astrophysical problem places on the complete range of possible PAH variants. In principle, the PAH molecular parameter space is effectively infinite, and the species studied to date probe only a subset of that parameter space. The possible variations on the current set of PAHs that might account for disparate spectroscopic characteristics can be grouped into two broad categories: larger and/or different PAH species and heteroatomic PAH variants.

5.1.1. Larger and/or Different PAH Species

There are essentially an infinite number of possible PAH structures that might exist in space. Thus, one might question whether larger PAHs or PAHs with some distinctive structural characteristic might also be able to account for the interstellar 6.215 μm emission component. However, this possibility seems unlikely for a couple of reasons. First, the spectroscopic studies of PAHs reported to date have explored the parameter space of PAH

structural characteristics reasonably thoroughly, including many different edge configurations, decoration with a variety of functional groups (Langhoff et al. 1998), and superhydrogenation of a portion of the aromatic network (i.e., H_nPAHs ; Schutte et al. 1993; Bernstein et al. 1996; Sloan et al. 1997). Second, a shift in the dominant emission band for species larger than those reflected in Figures 4 and 5 above would require the emergence of a new spectroscopic characteristic in a regime where those characteristics are expected to be *converging* (toward the infinite limit of the graphitic sheet) rather than *diverging*. Consequently, it does not seem likely that the shift is an artifact of molecular structure or size. Furthermore, the emission near 6.2 μm is dominated by PAHs containing less than 100 C atoms (Schutte et al. 1993).

5.1.2. Heteroatomic PAH Variants

Alternatively, one might question whether there are heteroatom variants other than those considered here that can accommodate the position of the class A 6.2 μm emission feature as well as endoskeletal PANH cations. To address this question, we must examine the constraints of the problem. First, we can rule out a large majority of the periodic table simply on the basis of chemical abundance. For reference, the abundances of the 10 most abundant, chemically reactive elements after hydrogen are given in Table 4, normalized to the abundance of C (values adapted from Spitzer 1978, p. 4). It is highly unlikely that elements with lower abundances than these could observably influence the global spectroscopic characteristics of the interstellar PAH population.

Second, since the studies presented above indicate that it is unlikely that metallocene complexes can reproduce the interstellar class A emission feature, the list of possible heteroatom substituents can be further pared down by restricting our consideration to only those elements capable of bonding covalently to the carbon skeleton of a PAH. Of the species in Table 4, only O, N, Si, and S satisfy this constraint. O and Si were ruled out by the results discussed in § 4, and S has both a low electronegativity and a limited valency, so it can be eliminated as well. Thus, PANH cations represent the only heteroatom variant of the PAH family that is feasible both with respect to cosmic abundances and with respect to the chemical constraints of the problem.

Consequently, although other possible origins for the position of the class A component of the interstellar 6.2 μm emission band cannot be unequivocally ruled out at this point, we believe that the computational studies discussed in § 4.3, together with the foregoing circumstantial arguments against other possible contributors, strongly favor endoskeletal PANH cations as the

TABLE 4
COSMIC ABUNDANCES OF THE 10 MOST ABUNDANT CHEMICALLY
REACTIVE ELEMENTS AFTER HYDROGEN

Element	Abundance Relative to C ^a
O.....	1.6
C.....	1.0
N.....	0.25
Mg.....	0.079
Si.....	0.079
Fe.....	0.063
S.....	0.040
Al.....	6.3×10^{-3}
Ca.....	6.3×10^{-3}
Na.....	5.0×10^{-3}

^a Values adapted from Spitzer (1978).

carrier of the interstellar band. Consequently, the class A component of the interstellar 6.2 μm emission band seems to provide a reliable indication that N is incorporated into the interstellar PAH population.

5.2. The 6.2 μm Emission Band: An Indicator of PAH Size and Nitrogen Content

It was shown in § 3.2.2 that the effect of the presence of a nitrogen atom in the interior of a PAH becomes diluted as the molecular size of the species increases. In coronene (24 C atoms), a single endoskeletal N atom was sufficient to shift the dominant CC stretching feature to 6.18 μm , the position needed to explain the class A emission component. Singly N-substituted ovalene (32 C atoms) came close to this position (6.20 μm), but circumcoronene (54 C atoms) required two endoskeletal N atoms to achieve a blueshift of this magnitude. This behavior, together with the position of the interstellar class A emission component, implies that the N/C ratio in the PANH cation population responsible for that feature must be no less than about $\sim 1/30$ and provides the basis for estimating the amount of cosmic N that is tied up in C-rich dust.

The interstellar PAH emission at 6.2 μm is believed to be dominated by species in the size range from 60 to 90 C atoms (Schutte et al. 1993). The results of the present study indicate that PANHs in this size range require at least 2–3 nitrogen atoms to reproduce the class A band position. Assuming, conservatively, that there are an average of three nitrogen atoms incorporated into the interstellar PAHs that dominate the emission spectrum at this wavelength and that the average size of the emitters is 90 C atoms (considering all of the mid-IR bands, not just the CC stretch component; Schutte et al. 1993), the amount of nitrogen tied up in PAHs must be at least 3% of the amount of carbon tied up in the PAHs to explain the position of the class A interstellar feature.

Now, the latest estimates (Snow & Witt 1995) place the amount of cosmic carbon tied up in PAHs at between 10% and 30%. Thus, assuming the lower limit of this range, we have

$$N_C^{\text{PAH}} = 0.10N_C,$$

where N_C^{PAH} is the amount of C locked up in PAHs and N_C is the cosmic abundance of C. Taking the conservative value of N/C = 3% in the PAH population from above, the amount of nitrogen tied up in the PAH population can be expressed as

$$N_N^{\text{PAH}} = 0.03N_C^{\text{PAH}} = 0.03(0.10N_C) = 0.003N_C.$$

Using this result, we can calculate the fraction of the cosmic nitrogen that is tied up in the interstellar PAH population,

$$\chi_N^{\text{PAH}} = \frac{N_N^{\text{PAH}}}{N_N} = \frac{0.003N_C}{0.25N_C} = 0.012,$$

where we have used the cosmic abundance of N relative to C from Table 4. Thus, the results of this study imply that at least 1.2% of the available cosmic N is tied up in the interstellar PAH population. It should also be emphasized that this is a conservative estimate. Within the uncertainties associated with the quantities that went into this calculation, the value could easily be as high as 5%–6% of the cosmic nitrogen, making the PAH population a significant reservoir of nitrogen in the interstellar medium.

5.3. Rotational Spectroscopy of Interstellar PANHs

As pointed out by Mattioda et al. (2003), by virtue of their permanent dipole moments, PANHs exhibit pure rotational

TABLE 5
CALCULATED DIPOLE MOMENTS FOR THE SINGLY SUBSTITUTED ISOMERS OF THE N-CORONENE, N-OVALENE, N-CIRCUMCORONENE, AND N-CIRCUM-CIRCUMCORONENE CATIONS

SPECIES	DIPOLE MOMENTS		
	μ_a (D)	μ_b (D)	μ (D)
N-coronene Cations			
1N.....	5.48	0.19	5.49
2N.....	3.69	0.00	3.69
3N.....	2.67	0.00	2.67
N-ovalene Cations			
1N.....	7.10	0.98	7.17
1'N.....	5.38	4.81	7.21
1''N.....	4.92	4.26	6.51
1'''N.....	0.00	3.47	3.47
2N.....	5.25	1.19	5.38
2'N.....	1.59	3.65	3.98
3N.....	4.32	1.02	4.44
3'N.....	1.29	1.99	2.37
4N.....	0.00	1.56	1.56
N-circumcoronene Cations			
1N.....	9.23	0.23	9.23
1'N.....	6.99	0.00	6.99
2N.....	6.77	0.47	6.79
3N.....	5.30	1.20	5.43
4N.....	4.55	0.00	4.55
5N.....	1.32	0.00	1.32
N-circum-circumcoronene Cations			
2N.....	10.12	0.33	10.13
2'N.....	9.09	0.00	9.09
3N.....	7.47	1.94	7.72
3'N.....	8.31	0.00	8.31
4N.....	7.33	0.63	7.72
5N.....	4.75	0.62	4.79
6N.....	3.06	0.00	3.06
7N.....	2.54	0.00	2.54

spectra and can, if present, contribute to the cosmic microwave emission. In view of this potential, the dipole moments and rotational constants have been calculated at the B3LYP/4-31G level of theory and are tabulated in Tables 5 and 6, respectively.

The majority of PANH species are asymmetric top molecules (i.e., the moments of inertia about each of the molecule's three internal coordinate axes are different). The rotational axes of each molecule are identified as a , b , and c on the basis of the moment of inertia, I , about each axis and according to the convention $I_a < I_b < I_c$. The rotational constants about the a , b , and c axes are denoted A , B , and C , respectively, and are determined by the standard expression,

$$Q = \frac{\hbar}{4\pi c I_q},$$

where Q ($= A, B$, or C) is the rotational constant and I_q is the moment of inertia about the q -axis.

The B3LYP dipole moments are computed at the center of mass of each molecule, with the a , b , and c (normal to the plane of the molecules) axes being the principal axes of inertia. For these planar species, the components of these dipole moments

TABLE 6

CALCULATED ROTATIONAL CONSTANTS FOR THE SINGLY SUBSTITUTED ISOMERS OF THE N-CORONENE, N-OVALENE, N-CIRCUMCORONENE, AND N-CIRCUM-CIRCUMCORONENE CATIONS

SPECIES	ROTATIONAL CONSTANTS		
	A (GHz)	B (GHz)	C (GHz)
N-coronenes	0.334–0.337	0.331–0.336	0.166–0.168
N-ovalenes	0.238	0.148	0.091
N-circumcoronenes	0.066	0.066	0.033
N-circum-circumcoronenes	0.021	0.021	0.011

are necessarily confined to the plane of the molecule, i.e., $\mu_c \equiv 0$ in all cases. For comparison, the values for smaller PANHs such as those shown in Table 1 can be found in Mattioda et al. (2003). Calibration calculations at the same level of theory for the benzene molecule yield rotational constants that are accurate to within 1%. Furthermore, the experimental (theoretical) dipole moments for CO, H₂CO, and HC₃N are 0.117 (0.158), 2.34 (2.45), and 3.6 (3.86) D, respectively. Thus, while the calculated rotational constants such as those listed in Table 6 are insufficient to calculate precise rotational line positions, they are sufficient to constrain the strengths and wavelength regions in which PANH rotational transitions are expected.

The rotational constants for the internally single N-substituted PANHs tabulated in Table 6 span the range from 0.34 to 0.01 GHz with dipole moments varying from 0 to nearly 10 D. In comparison, the rotational constants for the smaller PANHs considered in Mattioda et al. (2003) span the range from 1.6 to 0.2 GHz, and the dipole moments vary from 4.3 to 0 D. Given that PANHs larger than circumcoronene and probably approaching the size of circum-circumcoronene are likely in the interstellar medium (ISM), it is reasonable to extrapolate that the rotational constants for the majority of interstellar PANHs will be $\ll 1$ GHz, while their dipole moments may be as large as tens of debyes. Thus, if PANHs indeed dominate the PAH population, they could be an unrecognized but important contributor to Galactic and extragalactic microwave emission.

Given the enormous number of PANH structures possible, the vanishingly small rotational constants of PANHs the size of those that populate the ISM, and the likelihood that most cosmic PANHs will have multiple substituted N atoms, interstellar PANHs should produce a very dense forest of lines over a very broad spectral range. For example, a mixture of PANHs up to a size of circum-circumcoronene at 100 K are expected to emit in a pseudocontinuum between about 0 and 40 GHz. While such emission would be expected to be associated with regions that emit the unidentified infrared (UIR) emission features, it is also possible that microwave emission from rotationally excited PANHs could originate in low-radiation regions as well. Furthermore, given that these species are so widespread throughout the cosmos, it is also possible that they could superpose absorption structure against strong background radio and microwave continuum emission sources such as supernova remnants.

An interesting consequence of this is that PANHs may represent an important fraction of the “spinning ultrasmall” grain population proposed by Draine & Lazarian (1998a, 1998b) to account for the excess Galactic microwave emission at 14.5, 31.5, 32, and 53 GHz reported by Kogut et al. (1996), de Oliveira-Costa et al. (1997), and Leitch et al. (1997). These authors report a strong spatial correlation between this anomalous emission and the *Infrared Astronomical Satellite* (IRAS) 100 μ m

dust emission from high-latitude clouds. Not only is this 100 μ m emission strongly correlated with the PAH emission features, but the peak CC stretching band of those features falls close to 6.2 μ m, the position directly implicating large PANHs.

Given their large dipole moments, it may also be possible to distinguish the rotational emission lines of interstellar PANHs among the forest of molecular rotational lines observed in cold, dark molecular clouds. Rotational level populations should be low at the low ambient temperatures characteristic of such regions ($T_{\text{gas}} \approx 10$ K), thus simplifying the spectrum for an individual PANH by collapsing the emission into a relatively small number of transitions. Furthermore, it may be that among the PANH population there are some species that possess large dipole moments and have a high enough degree of symmetry that the number of substitutional isomers is sufficiently small that these species could have unusually intense radio lines. This is similar to the situation with the radio detection of the interstellar cyanopolyenes. Their detection is not so much a reflection of a chemistry that favors the production of these types of compounds over other organic compounds, but rather owes to the fact that this particular family of species has exceptionally high dipole moments and relatively small partition functions.

Complete and proper testing of this hypothesis will require a full quantum mechanical treatment of the rotational spectrum of a variety of singly and multiply N-substituted PANHs. As PANHs are asymmetric rotors, this is well beyond the scope of this paper.

5.4. Electronic Spectroscopy of Interstellar PANHs

Since nitrogen has one more electron than carbon, the substitution of a nitrogen atom for a carbon atom in the aromatic network can have a profound effect on the electronic transitions of the species in the UV/visible/NIR regions. As mentioned in § 3.1, since a N atom and a CH group are isoelectronic, substitution of a single N atom on the periphery of a PAH, forming an exoskeletal PANH, yields a neutral molecule with a closed-shell electronic structure whose corresponding cation will have an open-shell, radical structure. Thus, the electronic spectra of these species will resemble that of their neutral and cationic PAH counterparts, respectively. However, when the substitution of a single N atom (or, indeed, any odd number of N atoms) occurs at an endoskeletal position, the situation is reversed. Since an N atom has one more electron than does a C atom, it is the *neutral* endoskeletal PANH that has the open-shell structure, while the corresponding *cation* has the closed-shell structure. As we shall see, this difference in electronic structure has important implications for astrophysics.

The difference in the electronic spectroscopy of PAHs and endoskeletal PANHs can be illustrated by comparing circumcoronene and 5N-circumcoronene (structures shown in Fig. 2). The time-dependent (Stratmann et al. 1998) B3LYP/4-31G excitation energies and oscillator strengths for the lowest electronic excited states of circumcoronene, circumcoronene cation, 5N-circumcoronene, and 5N-circumcoronene cation are given in Table 7. The B3LYP/4-31G energy levels of the highest occupied and lowest unoccupied orbitals of these four systems are shown in Figure 6. The lowest lying electronic transitions in each case are indicated by the vertical bars in the diagram. The numbering of the transitions is in order of increasing energy and corresponds to the numbering of the rows in Table 7. This level of theory has been shown (Hirata et al. 2003) to yield excitation energies accurate to about ± 0.3 eV and oscillator strengths that are consistent with experiment. This level of accuracy is sufficient to illustrate the differences between the PAHs and PANHs.

TABLE 7
TD-B3LYP EXCITATION ENERGIES Δ IN eV AND OSCILLATOR STRENGTHS f OF THE LOWEST ELECTRONIC EXCITED STATES OF CIRCUMCORONENE, CIRCUMCORONENE CATION, 5N-CIRCUMCORONENE, AND 5N-CIRCUMCORONENE CATION

STATE	CIRCUMCORONENE (NEUTRAL, CLOSED SHELL)		CIRCUMCORONENE ⁺ (CATION, OPEN SHELL)		5N-CIRCUMCORONENE ⁺ (CATION, CLOSED SHELL)		5N-CIRCUMCORONENE (NEUTRAL, OPEN SHELL)	
	Δ (eV)	f	Δ (eV)	f	Δ (eV)	f	Δ (eV)	f
1.....	2.29	0.000	0.14 ^a	0.000	2.06	0.068	0.52 ^b	0.003
2.....	2.46	0.000	1.10 ^a	0.025	2.19	0.048	0.99 ^b	0.000
3.....	2.98	1.002	1.11 ^a	0.021	2.65	0.197	1.30 ^b	0.007
4.....	2.98	1.003	1.16 ^a	0.099	2.72	0.434	1.54 ^b	0.016
5.....	3.21	0.000	1.77 ^a	0.023	2.95	0.394	1.69 ^b	0.036
6.....	1.86 ^b	0.022	1.89 ^a	0.006

^a Corresponds to a transition from a closed-shell to an open-shell orbital.

^b Corresponds to a transition from an open-shell orbital to a virtual orbital.

In Figure 6, the orbital energies of neutral circumcoronene correspond to the case labeled “closed 1.” Clearly, the lowest electronic excited states correspond to excitations from the highest occupied orbitals into the lowest unoccupied (virtual) orbitals. Since the gap between the occupied and unoccupied levels is relatively large, the smallest excitation energy is on the order of 2 eV ($\lambda \sim 600$ nm). The circumcoronene cation, on the other hand, has one fewer electron and corresponds to the case labeled “open 1.” Here the lowest energy transitions fall into two classes: (1) transitions from the highest doubly occupied, closed-shell orbitals to the singly occupied orbital and (2) transitions from the singly occupied orbital to higher lying virtual

orbitals. Both of these classes of transition are illustrated in Figure 6. In the case of the circumcoronene cation, we find that the lowest energy transitions fall into the first of the above two categories. Since the spacing between these occupied orbitals is relatively small, the excitation energies of the cation are much smaller than for the neutral, and the first six excited states of the cation are all at lower energies than for the neutral. An experimental study of these types of transitions in PAH radical cations has been reported by Mattioda et al. (2005).

As noted above, the situation is reversed in the endoskeletal PANH species. The 5N-circumcoronene cation is a closed-shell system, and its energy levels are described by the case labeled “closed 2.” Because of its closed-shell structure, the electronic transitions in this species correspond to excitations from doubly occupied orbitals to virtual orbitals, and the corresponding excitation energies are much more similar to those of the closed-shell neutral circumcoronene than the open-shell circumcoronene cation. Neutral 5N-circumcoronene, on the other hand, has one more electron than the closed-shell case, and its orbital energies are described by the case labeled “open 2.” As was the case for the open-shell circumcoronene cation, the electronic transitions in the neutral 5N-circumcoronene radical fall into the two classes described above. In this case, however, it is the excitations from the highest occupied orbital into the lowest unoccupied orbital that are lowest in energy. This difference can be traced to the fact that, compared to the corresponding closed-shell species, the circumcoronene radical cation is created by *removing* an electron from a bonding molecular orbital, while the 5N-circumcoronene radical (neutral) is formed by *adding* an electron to an unoccupied antibonding orbital. Inspection of the excitation energies in Table 7 shows that the electronic spectrum of 5N-circumcoronene is more similar to that of the circumcoronene cation than to that of circumcoronene.

This reversal of neutral/cation spectroscopic character may hold the key to understanding one of the principal challenges currently facing the hypothesis that the absorptions of members of the interstellar PAH family are responsible for the enigmatic visible/NIR diffuse interstellar bands (DIBs). Sensitive observations returned by such platforms as the Infrared Telescope in Space (IRTS), *ISO*, and the *Spitzer Space Telescope* consistently show that the infrared spectrum emitted by dust in the diffuse ISM has the characteristics of PAH cations—that is, the features at 6.2, 7.7, and 8.6 μm dominate those at 11.2 and 3.3 μm (e.g., Onaka et al. 1996). Within the framework of the PAH model, this infrared emission is pumped by absorbed photons from the diffuse interstellar radiation field—including the DIB absorptions.

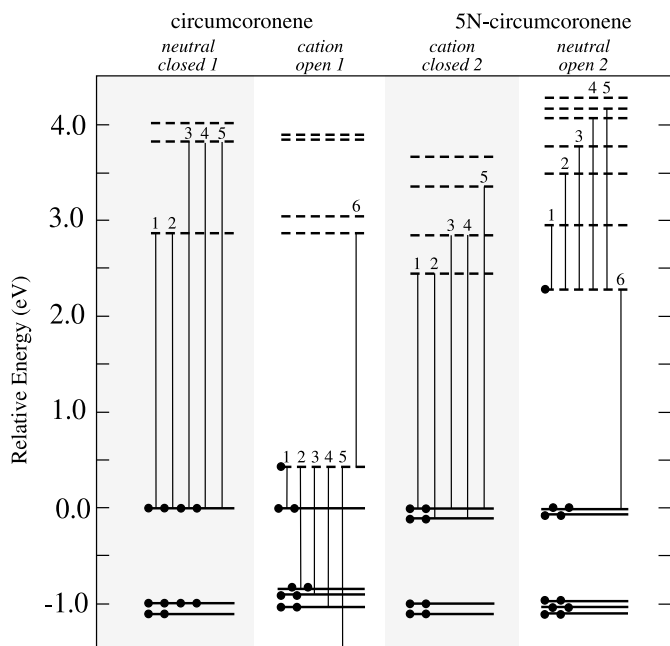


FIG. 6.—Calculated B3LYP/4-31G orbital energy levels for the neutral and cationic forms of circumcoronene and 5N-circumcoronene. The orbital energies are shifted so that the highest doubly occupied orbital is at 0.0 eV. The dots indicate the electrons occupying each energy level. Some of the circumcoronene neutral orbitals are doubly degenerate, so they can contain four electrons. The vertical bars indicate the possible transitions and are numbered from least to greatest in accordance with Table 7. For the open-shell species, six excitations are shown to illustrate the two classes of possible excitations: open-shell to virtual orbital and doubly occupied to singly occupied orbital. Note that because the TD-DFT approach accounts for many high-order effects, the transition energies in Table 7 do not, in general, correspond to differences in orbital energies shown in the plot.

Surprisingly, the characteristics of those absorption features seem to tell a different story. The latest experimental studies of cold, gas-phase PAHs and PAH cations reveal that neutral (i.e., closed shell) PAHs exhibit electronic absorption line widths that are consistent with those observed for the majority of the DIBs (ca. 3 cm^{-1} ; Tan & Salama 2005), while PAH radical cations exhibit line widths that are far broader (i.e., $20\text{--}30 \text{ cm}^{-1}$) than the typical DIB (Biennier et al. 2003; Sukhorukov et al. 2004; Zhao et al. 2004). This striking difference can be traced to differences in the intrinsic lifetimes of the excited states accessed by electronic absorptions in the closed-shell (neutral) and open-shell (radical cation) species. Thus, the characteristics of the absorbed visible/NIR features seem to tell a different story about the carriers than do the emitted IR features.

However, endoskeletal PANH species may provide a solution to this apparent conundrum. In endoskeletal PANHs, as we have seen, it is the cationic species that have the closed-shell structure, while the neutrals have the open-shell, radical electronic structure. Thus, while the IR spectrum of these species will exhibit the general characteristics associated with PAH cations, the electronic absorption spectrum should be expected to exhibit the characteristics (i.e., relatively narrow line widths) of a closed-shell species. Thus, PANH cations sufficiently large to produce absorptions in the visible/NIR regions can accommodate both the characteristic profiles of the DIB absorptions and the cationic character of the resulting cirrus emission.

As in § 5.3, complete and proper testing of this aspect of the PANH hypothesis will require a full quantum mechanical treatment of the electronic properties of a variety of singly and multiply N-substituted PANHs.

6. CONCLUSIONS

The peak wavelength of the dominant CC stretching feature near $6.2 \mu\text{m}$ decreases steadily with molecular size at the small end of the PAH cation size distribution (ca. $10\text{--}30$ C atoms), leveling off at about $6.3 \mu\text{m}$ for species with more than about $30\text{--}40$ carbon atoms. While this could account for the longest wavelength observed ($6.3 \mu\text{m}$) for the interstellar $6.2 \mu\text{m}$ feature, it could not account for the shortest observed wavelength ($6.22 \mu\text{m}$).

This failure to match the short-wavelength component motivated this study, where we computationally investigated several molecular parameters that one can reasonably anticipate will vary under astronomical conditions and might alter vibrational mode frequencies within a family of molecules such as the PAHs. The most important include size, structure, heteroatom substitution of a ring carbon, complex formation, and multiple charge. Each of these has been considered here. While the overall spectra are similar for all of these variations and show that they all belong to the PAH family, only N atom substitution induced a shift of the CC stretch to the observed $6.22 \mu\text{m}$ position.

The calculations seem to rule out oxygen or silicon atom substitution, metal cation complex formation, low PAH molecular symmetry, or multiple charge as being important in shifting the CC stretch wavelength to that observed for UIR bands. Other substitutions would appear to be ruled out as well based on either cosmic abundance constraints or the inability to fully participate in the PAH aromaticity. It appears that nitrogen substitution within the aromatic hexagonal network is unique in its ability to shift the CC stretch frequency into agreement with the observations.

The calculations show that the shortest wavelength of the interstellar $6.2 \mu\text{m}$ feature observed can only be reproduced by the aromatic CC stretch for large PAHs with nitrogen deep within

their structure, not with nitrogen in the outer rings. Substitution as a function of distance from the outer edge is the critical feature in understanding the shortest observed wavelength peak position of the $6.2 \mu\text{m}$ feature.

Thus, the interstellar $6.2 \mu\text{m}$ feature peak position appears to be a tracer of nitrogen tied up in PAHs. If this is borne out, then we have the following results:

1. A conservative lower limit of 1.2% of the cosmic nitrogen is tied up in PAHs.
2. The emitting PAH population in ISM-like sources (H II regions), most post-asymptotic giant branch (AGB) stars, and a few planetary nebulae (PNe) is dominated by large ($N_C \geq 50$ C atoms), N-substituted PANHs containing nitrogen within their framework.
3. In contrast, smaller PAHs ($N_C \leq 50$ C atoms), with N distributed evenly out to the periphery, dominate the emitting PANH population in most PNe, several isolated Herbig Ae-Be stars, and a few post-AGB stars.
4. PANHs possess permanent dipole moments and exhibit strong transitions in the microwave wavelength region. Thus, they will contribute to the cosmic microwave radiation and may be important components of the carriers of the anomalous background emission. Given the large number of PANH isomers possible, it is likely that the rotational lines will blend to produce a broad, continuous emission. In a few favorable cases, specific molecular identifications may be possible.
5. Neutral endoskeletal PANHs containing an odd number of N atoms are open-shell species and possess low-lying electronic transitions. These transitions in neutral PANHs span the visible and near-IR, as do the transitions in the open-shell PAH cations studied to date. This will modify our understanding of the IR emission process, as these neutral PANHs can contribute to the IR emission. Furthermore, if PANHs are present in the diffuse ISM, these open-shell neutral species can absorb at discrete wavelengths and contribute to the DIBs and other structure in the extinction curve.

The clear conclusion to be drawn from the above results is that nitrogen substitution, coupled with increasing PANH size, seems unique in its ability to reproduce the $6.2\text{--}6.3 \mu\text{m}$ range observed for the CC stretching feature. *Given this, and that nitrogen incorporation should naturally occur in the circumstellar birthplaces of these PAHs as they are formed, it is our opinion that most of the species responsible for the UIR spectrum contain nitrogen, and that the peak position of the interstellar CC stretching feature near $6.2 \mu\text{m}$ traces emitting PANH size and its nitrogen concentration.*

The authors gratefully acknowledge the sustained support from NASA's Exobiology and Long Term Space Astrophysics (LTSA) programs (UPNs 344-58-21 and 399-20-40), which made this work possible. We especially thank Els Peeters and Xander Tielens for bringing the variations in the CC stretching feature to our attention and many subsequent discussions, Andy Mattioda for helpful discussions concerning laboratory-measured PANH spectra, Duane Carbon for detailed discussions on late-type stellar mass loss, and Xiaofeng Tan and Jan Cami for discussions about the bandwidths of transitions between electronic states in neutral and ionized PAHs. Finally, we also thank the anonymous referee for a number of insightful suggestions that were helpful in improving this manuscript.

REFERENCES

- Allamandola, L. J., Hudgins, D. M., & Sandford, S. A. 1999, *ApJ*, 511, L115
- Allamandola, L. J., Tielens, A. G. G. M., & Barker, J. R. 1985, *ApJ*, 290, L25
- . 1989, *ApJS*, 71, 733
- Bakes, E. L. O., Tielens, A. G. G. M., & Bauschlicher, C. W. 2001, *ApJ*, 556, 501
- Basile, B. P., Middleditch, B. S., & Oró, J. 1984, *Organic Geochem.*, 5, 211
- Bauschlicher, C. W., Jr., & Bakes, E. L. O. 2000, *Chem. Phys.*, 262, 285
- Bauschlicher, C. W., Jr., & Langhoff, S. R. 1997, *Spectrochim. Acta A*, 53, 1225
- Becke, A. D. 1993, *J. Chem. Phys.*, 98, 5648
- Bernstein, M. P., Sandford, S. A., & Allamandola, L. J. 1996, *ApJ*, 472, L127
- Biennier, L., Salama, F., Allamandola, L. J., & Scherer, J. J. 2003, *J. Chem. Phys.*, 118, 7863
- Bregman, J., & Temi, P. 2005, *ApJ*, 621, 831
- Brenner, J. D., & Barker, J. R. 1992, *ApJ*, 388, L39
- Buchanan, J. W., Reddic, J. E., Grieves, G. A., & Duncan, M. A. 1998, *J. Phys. Chem. A*, 102, 6390
- Cernicharo, J., Yamamura, I., Gonzalez-Alfonso, E., De Jong, T., Heras, A., Escribano, R., & Ortigoso, J. 1999, *ApJ*, 526, L41
- Charmley, S. B., Ehrenfreund, P., & Kwan, Y.-J. 2001, *Spectrochim. Acta A*, 57, 685
- Cherchneff, I. 1996, in *IAU Symp. 178, Molecules in Astrophysics: Probes and Processes*, ed. E. van Dishoek (Cambridge: Cambridge Univ. Press), 469
- Cherchneff, I., & Barker, J. R. 1989, *ApJ*, 341, L21
- Colangeli, L., Mennella, V., & Bussoletti, E. 1992, *ApJ*, 385, 577
- Cook, D. J., & Saykally, R. J. 1998, *ApJ*, 493, 793
- Cox, P., & Kessler, M. F., eds. 1999, *The Universe as Seen by ISO*, Vol. II (ESA SP-427; Noordwijk: ESA)
- de Oliveira-Costa, A., Kogut, A., Devlin, M. J., Netterfield, C. B., Page, L. A., & Wollack, E. J. 1997, *ApJ*, 482, L17
- Draine, B. T., & Lazarian, A. 1998a, *ApJ*, 494, L19
- . 1998b, *ApJ*, 508, 157
- Draine, B. T., & Li, A. 2001, *ApJ*, 551, 807
- Flickinger, G. C., Wdowiak, T. J., & Gomez, P. L. 1991, *ApJ*, 380, L43
- Frenklach, M., & Feigelson, E. D. 1989, *ApJ*, 341, 372
- Frisch, M. J., Pople, J. A., & Binkley, J. S. 1984, *J. Chem. Phys.*, 80, 3265
- Frisch, M. J., et al. 1998, *Gaussian 98* (ver. A.11; Pittsburgh: Gaussian)
- Hayatsu, R., & Anders, E. 1981, *Top. Curr. Chem.*, 99, 1
- Hayatsu, R., Matsuoka, S., Scott, R. G., Studier, M. H., & Anders, E. 1977, *Geochim. Cosmochim. Acta*, 41, 1325
- Hirata, S., Head-Gordon, M., Szczepanski, J., & Vala, M. 2003, *J. Phys. Chem. A*, 107, 4940
- Hony, S., Van Kerckhoven, C., Peeters, E., Tielens, A. G. G. M., Hudgins, D. M., & Allamandola, L. J. 2001, *A&A*, 370, 1030
- Hudgins, D. M., & Allamandola, L. J. 1995, *J. Phys. Chem. A*, 99, 3033
- . 1997, *J. Phys. Chem. A*, 101, 3472
- . 1999, *ApJ*, 513, L69
- Hudgins, D. M., Bauschlicher, C. W., Jr., & Allamandola, L. J. 2001, *Spectrochim. Acta A*, 57, 907
- Hudgins, D. M., Bauschlicher, C. W., Jr., Allamandola, L. J., & Fetzer, J. C. 2000, *J. Phys. Chem. A*, 104, 3655
- Joblin, C., Boissel, P., Leger, A., d'Hendecourt, L. B., & Defourneau, D. 1995, *A&A*, 299, 835
- Jochims, H. W., Baumgartel, H., & Leach, S. 1999, *ApJ*, 512, 500
- Keller, R. 1987, in *Polycyclic Aromatic Hydrocarbons and Astrophysics*, ed. A. Leger, L. d'Hendecourt, & N. Boccarda (Dordrecht: Reidel), 387
- Kim, H., & Saykally, R. J. 2002, *ApJS*, 143, 455
- Klotz, A., Marty, P., Boissel, P., Serra, G., Chaudret, B., & Daudey, J. P. 1995, *A&A*, 304, 520
- Kogut, A., Banady, A. J., Bennett, C. L., Gorski, K. M., Hinshaw, G., & Reach, W. T. 1996, *ApJ*, 460, 1
- Langhoff, S. R. 1996, *J. Phys. Chem.*, 100, 2819
- Langhoff, S. R., Bauschlicher, C. W., Jr., Hudgins, D. M., Sandford, S. A., & Allamandola, L. J. 1998, *J. Phys. Chem. A*, 102, 1632
- Leitch, E. M., Readhead, A. C. S., Pearson, T. J., & Myers, S. T. 1997, *ApJ*, 486, L23
- Li, A., & Draine, B. T. 2001, *ApJ*, 554, 778
- Mattioda, A. L., Hudgins, D. M., & Allamandola, L. J. 2005, *ApJ*, 629, 1188
- Mattioda, A. L., Hudgins, D. M., Bauschlicher, C. W., Jr., Rosi, M., & Allamandola, L. J. 2003, *J. Phys. Chem. A*, 107, 1486
- Onaka, T., Yamamura, I., Tanabe, T., Roellig, T. L., & Yuen, L. 1996, *PASJ*, 48, L59
- Oomens, J., Tielens, A. G. G. M., Sartakov, B. G., von Helden, G., & Meijer, G. 2003, *ApJ*, 591, 968
- Pech, C., Joblin, C., & Boissel, P. 2002, *A&A*, 388, 639
- Peeters, E., Hony, S., Van Kerckhoven, C., Tielens, A. G. G. M., Allamandola, L. J., Hudgins, D. M., & Bauschlicher, C. W. 2002, *A&A*, 390, 1089
- Puget, J. L., & Leger, A. 1989, *ARA&A*, 27, 161
- Ricca, A., Bauschlicher, C. W., & Bakes, E. L. O. 2001a, *Icarus*, 154, 516
- Ricca, A., Bauschlicher, C. W., & Rosi, M. 2001b, *Chem. Phys. Lett.*, 347, 473
- Schutte, W. A., Tielens, A. G. G. M., & Allamandola, L. J. 1993, *ApJ*, 415, 397
- Senapati, L., Nayak, S. K., Rao, B. K., & Jena, P. 2003, *J. Chem. Phys.*, 118, 8671
- Serra, G., Chaudret, B., Saillard, Y., Le Beuze, A., Rabaa, H., Ristorcelli, I., & Klotz, A. 1992, *A&A*, 260, 489
- Sloan, G. C., Bregman, J. D., Geballe, T. R., Allamandola, L. J., & Woodward, C. E. 1997, *ApJ*, 474, 735
- Sloan, G. C., Hayward, T. L., Allamandola, L. J., Bregman, J. D., DeVito, B., & Hudgins, D. M. 1999, *ApJ*, 513, L65
- Snow, T. P., & Witt, A. N. 1995, *Science*, 270, 1455
- Spitzer, L., Jr. 1978, *Physical Processes in the Interstellar Medium* (New York: Wiley)
- Stephens, P. J., Devlin, F. J., Chabalowski, C. F., & Frisch, M. J. 1994, *J. Phys. Chem.*, 98, 11623
- Stratmann, R. E., Scuseria, G. E., & Frisch, M. J. 1998, *J. Chem. Phys.*, 109, 8218
- Sukhorukov, O., Staicu, A., Diegel, E., Rouillé, G., Henning, T., & Huisken, F. 2004, *Chem. Phys. Lett.*, 386, 259
- Szczepanski, J., Drawdy, J., Wehlburg, C., & Vala, M. 1995, *Chem. Phys. Lett.*, 245, 539
- Tan, X., & Salama, F. 2005, *J. Chem. Phys.*, 122, 084318
- Vala, M., Szczepanski, J., Pauzat, F., Parisel, O., Talbi, D., & Ellinger, Y. 1994, *J. Phys. Chem.*, 98, 9187
- Verstraete, L., et al. 2001, *A&A*, 372, 981
- Weilmunster, P., Keller, A., & Homann, K.-H. 1999, *Combustion Flame*, 116, 62
- Zhao, L., Lian, R., Shkrob, I. A., Crowell, R. A., Pommeret, S., Chronoster, E. L., Liu, A. D., & Trifunac, A. D. 2004, *J. Phys. Chem. A*, 108, 25